Polymer dynamics including side group motion: Free draining limit

Ronald S. Adler and Karl F. Freed

Citation: The Journal of Chemical Physics **72**, 2032 (1980); doi: 10.1063/1.439352
View online: http://dx.doi.org/10.1063/1.439352
View Table of Contents: http://scitation.aip.org/content/aip/journal/jcp/72/3?ver=pdfcov
Published by the AIP Publishing

Polymer dynamics including side group motion: Free draining limit

Ronald S. Adler and Karl F. Freed

The James Franck Institute and The Department of Chemistry, The University of Chicago, Chicago, Illinois 60637

(Received 17 January 1979; accepted 30 April 1979)

We present an exactly soluble model of polymer chain dynamics in which the effects of side group interactions are explicitly treated. Calculations for the relaxation spectrum, intrinsic viscosity, $[\eta(\omega)]$, and dielectric dispersion for both longitudinal and perpendicular dipole moments are presented in the free draining limit. Perpendicular dipoles are described by attaching a dipole moment to each side group. The relaxation spectrum displays two branches corresponding to local and global chain motions, the latter being highly depressed. The low frequency behavior of $[\eta(\omega)]$ and of longitudinal dipoles is shown to be well represented by an effective Rouse model, whereas $[\eta(\omega)]$ displays a plateau, $[\eta]_\infty$, at higher frequencies which is (i) not associated with the gap in the relaxation spectrum, (ii) independent of molecular weight for long enough chains, and (iii) correlated to the degree of side group motional freedom in accordance with experiment. For short chains the plateau region $[\eta]_\infty$ vanishes, and the model displays a molecular weight dependence. The relaxation of perperdicular dipoles is demonstrated to be independent of molecular weight for long enough chains. For shorter chains, however, global chain motions (e.g., overall rotation) significantly affect the behavior of the dielectric loss. Our model is shown to reproduce the phenomenological model of Dubois–Violette *et al.* and of Stockmayer *et al.* which has been used to rationalize the perpendicular dipole dielectric data. Furthermore, we show how our model and generalizations thereof can be derived from a true molecular model with realistic bonding and nonbonding interactions using the Zwanzig–Mori projection operatior formalism.

I. INTRODUCTION

The low frequency dynamical behavior of a polymer solution at infinite dilution is well represented in terms of the Rouse–Zimm theory.[1–3] In this theory, a polymer molecule is represented as a connected sequence of statistical units, each unit being characterized by an effective size and friction coefficient. Hydrodynamic interactions are incorporated through the preaveraged Oseen tenson.

Experimental data for the high frequency behavior of a polymer solution, however, display a marked departure from the predicted Rouse–Zimm behavior.[4,5] These data indicate the presence of a high frequency plateau $[\eta]_\infty$ (absent in the Rouse–Zimm theory) in the frequency dependent intrinsic viscosity $[\eta(\omega)]$, which is about one to two orders of magnitude smaller than $[\eta(0)]$. $[\eta]_\infty$ is also observed to be independent of molecular weight for long enough chains (e.g., $M \gtrsim 10^4$ for polystyrene) and to be correlated with the degree of side chain flexibility.[5] Evidently, this behavior is somehow attributable to local degrees of freedom within a chain, although the actual molecular mechanisms that give rise to $[\eta]_\infty$ are still not clearly understood.

One proposed method of rationalizing the presence of $[\eta]_\infty$ is to introduce the notion of internal viscosity, first suggested by Kuhn and Kuhn.[6] This idea has since been elaborated upon theoretically by Cerf and Peterlin,[7,8] who introduce a phenomenological model which is appealing because of its mathematical simplicity. Although the physical concepts motivating the introduction of internal viscosity are quite reasonable, the microscopic origins, enabling evaluation of the internal viscosity (along with its mode and frequency dependence) from the microscopic interaction potentials, etc., have remained an enigma. Adelman and Freed[9] have shown the relationship of internal viscosity of the memory terms which arise from internal friction forces that are due to the following:

(i) the replacement of actual intermononomer interactions by bead–spring forces, and/or

(ii) by considering the dynamics of a subset of all the degrees of freedom.

Recent calculations, which attempt to fit the Cerf–Petelin[8] theory to the observed viscoelastic data using exact Rouse–Zimm eigenvalues, have not been totally successful.[5] The difficulty apparently lies in the mode dependence assigned to the internal viscosity by the Cerf–Petelin theory. It is of interest to approach the problem of high frequency polymer dynamics from a somewhat more fundamental point of view to attempt to clarify the molecular mechanisms for the observed behavior.

Theoretical treatments of polymer dynamics, using fixed bond lengths and possibly bond angles, have resulted in calculated values of $[\eta]_\infty$ which are several orders of magnitude too small.[9–11] Hence, these constraints cannot be responsible for the observed $[\eta]_\infty$. Recent Monte Carlo calculations by Fixman[12] for Rouse chains with fixed bond lengths and angles as well as hindered bond rotations demonstrate that the latter feature can produce an $[\eta]_\infty$ of the correct qualitative form.

Similar departures from predicted Rouse model behavior are noted in the high frequency ($\sim 10^9$ Hz) dielectric dispersion of perpendicular dipole moments situated along a chain backbone.[13] The rate at which this relaxation occurs is observed to be independent of molecular weight for sufficiently long chains, indicating that only local properties are involved. Dubois-Violette and coworkers[14,15] and Stockmayer *et al.*[16] have shown that the

 0021-9606/80/032032-18$01.00

high frequency dielectric data is satisfactorily explained (for large molecular weights) by a shifted Rouse model. In the latter, local effects are incorporated phenomenologically into the Rouse model by the addition of a mode independent loss mechanism. The molecular weight dependence, which enters at lower molecular weights, is interpreted by Stockmayer *et al.* as arising from the overall rotational motion of the polymer whose relaxation time has now become comparable to the modeled local ones.[13]

In order to further understand the molecular origins of $[\eta]_\infty$ and of the dielectric dispersion data, we investigate an exactly solvable model[17] of polymer chain dynamics with the following important features:

(i) The model is of a bead–spring type and hence retains the simplicity of the Rouse–Zimm theory.

(ii) Side group motions are explicitly incorporated through the use of additional Rouse units to represent the side groups.

(iii) Hindered rotational potentials are simulated by side group–side group interactions.

(iv) Constaints on bond lengths and backbone bond angles are ignored consistent with their minor influence on $[\eta]_\infty$.

(v) Additional constraints which set up the local geometry between side groups and their neighboring bond vectors are easily incorporated into the model. One such constraint that is considered specifies the preferred orientation of a side group relative to its two adjacent bond vectors.

The model is solved in the free draining limit as this case permits closed analytic expressions to be given for various correlation functions of interest. The inclusion of hydrodynamic interactions will be considered in a subsequent paper.[18]

In the section to follow, the model is described, and the basic equations of motion are presented. As demonstrated by Zwanzig and Bixon,[19,20] using projection operator techniques, Rouse-like theories of polymer dynamics may be constructed rigorously from realistic intermonomer potentials when the higher frequency effects of the memory terms are ignored. In Appendix A, we show that our model may similarly be derived from a realistic true molecular model which involves all of the individual atomic centers and specific bonded and nonbonded interactions.

A solution of the model equations of motion is presented in Sec. III. We demonstrate that the relaxation rates of fundamental modes $\{\lambda_{k\alpha}\}$ satisfy a complicated transcendental equation which contains effects due to the boundary conditions at the ends of the chain. This complication is circumvented by systematically treating these end effects as a perturbation. Analytical expressions are given for the approximate $\{\lambda_{k\alpha}\}$ in terms of Rouse eigenvalues[1] and the end corrections are evaluated and are shown to be $O(N^{-1})$. The resulting modes display two branches similar to those discussed by Fixman and Evans.[21] The lower branch, which corresponds to collective chain motions, is greatly depressed from the usual Rouse-like behavior in qualitative agreement with Fixman's calculations.[12]

Starting with the linear response theory formulation of the intrinsic viscosity[22] and the eigenspectrum $\{\lambda_{k\alpha}\}$, $[\eta(\omega)]$ is calculated in Sec. IV. We present numerical calculations for a set of model parameters. Our results indicate that the model displays a first plateau of a relative magnitude to $[\eta(0)]$ and at a reduced frequency which is comparable to experimental values of $[\eta]_\infty$. Hence, we associate this plateau with the experimental $[\eta]_\infty$ and henceforth refer to the former as $[\eta]_\infty$. For large side groups (the only situation considered experimentally to date[5]), the model gives values of $[\eta]_\infty/[\eta(0)]$ of a reasonable order of magnitude. The model and a prediction of a plateau region $[\eta]_\infty$ are likewise valid for small side groups. A closed analytic expression for $[\eta(\omega)]$ is given from which $[\eta]_\infty$ is estimated. The calculated $[\eta]_\infty$ is *not* associated with the gap between the two branches of the relaxation rates, and $[\eta]_\infty$ emerges due to the hindered rotation potentials which are simulated through the side group–side group interactions. The gap appears at considerably higher frequencies than the plateau region for $[\eta]_\infty$. For certain values of the model parameters, this gap produces a second higher frequency plateau region for the viscosity several orders of magnitude smaller than $[\eta]_\infty$. The value of $[\eta]_\infty$ is, furthermore, independent of whether the interaction between side groups tends to align them into isotactic or syndiotactic configurations. The independence of $[\eta]_\infty$ on molecular weight for long enough chains is demonstrated. For short chains (≤ 100 units), the first plateau region vanishes, and the behavior of $[\eta(\omega)]$ is characterized by the same mechanism that gives rise to $[\eta]_\infty$. Comparisons are also made to an effective Rouse model whose parameters are chosen to simulate the low frequency spectrum of $[\eta(\omega)]$.

The behavior of the dielectric susceptibility is considered in Sec. V. The relaxation of the total longitudinal and perpendicular dipole moments are treated separately. The former conforms to the usual Rouse-like behavior in terms of the effective Rouse model (Sec. IV) apart from corrections at high frequencies. The latter displays a rapid decay which is independent of molecular weight for long enough chains and exhibits a molecular weight dependence for short chains related to global chain motions in agreement with experiment.[13] Perpendicular dipole moments are explicitly treated by assigning a dipole moment to each side group. A similar treatment of perpendicular dipoles has been considered by Shore and Zwanzig.[23] However, they consider dipoles attached to a one dimensional lattice, thereby restricting the validity of their approach to high frequencies and long chains. Numerical calculations are presented for both the real and imaginary parts of the dielectric susceptibility. Closed analytic expressions are also given for the autocorrelation functions of the total longitudinal and perpendicular dipoles moments. These expressions allow for comparison between model parameters with those of a shifted Rouse model.[14] The close agreement between the two models provides a re-

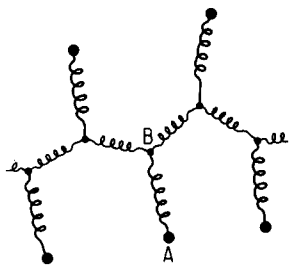

FIG. 1. Representation of the Rouse-like model in which side groups and backbone units are designated as A and B, respectively. Hindered rotational potentials are given in terms of AB–AB bond interactions. Additional interactions between A_iB_i and B_iB_i bonds yield preferred side group–backbone bond angles.

lationship between their respective parameters and a demonstration that the predictions of our model are in general agreement with experiment.

In Sec. VI, we consider a simple generalization of the model in which each side group is allowed to interact with its two adjacent bond vectors. This interaction tends to orient a side group to lie in a plane perpendicular to the chain axis at its location. Such interactions are expected to be more representative of actual chain geometries, and they enhance the hinderance to free rotation of the side groups. Results are presented graphically for both the intrinsic viscosity and dielectric susceptibility. Our calculations indicate that this increase in the hindered-rotation potential yields a more pronounced plateau region in $[\eta(\omega)]$. No significant changes are noted in the dielectric dispersion when these additional interactions are introduced.

II. DESCRIPTION OF MODEL

The model we propose is depicted in Fig. 1. We consider a chain consisting of $N+1$ backbone units, denoted as B units, that are connected harmonically and characterized by a Kuhn length σ_B. Attached to each B unit is an A unit which represents a side group.[24] The configurational free energy for this chain is taken to be

$$U=\frac{3k_BT}{2\sigma_B^2}\left\{\sum_{i=0}^{N-1}|\mathbf{x}_{i+1}-\mathbf{x}_i|^2+\epsilon_1\sum_{i=0}^{N}|\mathbf{x}_i-\mathbf{y}_i|^2+\epsilon_2\sum_{i=0}^{N-1}(\mathbf{x}_{i+1}-\mathbf{y}_{i+1})\cdot(\mathbf{x}_i-\mathbf{y}_i)\right\},\quad \epsilon_1>0\,, \tag{2.1}$$

where k_BT is the temperature in units of energy, and the sets $\{\mathbf{x}_i\}$ and $\{\mathbf{y}_i\}$ represent the position coordinates of B units and A units, respectively. Equation (2.1) would reduce to Kastner's model[25] of a Rouse comb-like chain if ϵ_2 were set equal to zero. In this case, the effective Kuhn length of an A–B unit is given by $\sigma_B/\sqrt{\epsilon_1}$.

For nonzero values of ϵ_2 the term

$$\epsilon_2\sum_{i=0}^{N-1}(\mathbf{x}_{i+1}-\mathbf{y}_{i+1})\cdot(\mathbf{x}_i-\mathbf{y}_i)$$

simulates hindered rotational potentials in a chain. The degree of side chain freedom of motion is determined by the magnitude of the parameter $3k_BT\epsilon_2/2\sigma_B^2$, whereas the sign of ϵ_2 determines whether the preferred alignment of side groups tends to be isotactic ($\epsilon_2<0$) or syndiotactic ($\epsilon_2>0$).

In the free draining limit, and neglecting inertia, we can write the following equation of motion for the set $\{\mathbf{x}_i,\mathbf{y}_i\}_{i=0,1,\ldots,N}$:

$$\frac{d}{dt}\mathbf{x}_i(t)=\zeta_B^{-1}\mathbf{F}_{Bi}\,, \tag{2.2a}$$

$$\frac{d}{dt}\mathbf{y}_i(t)=\zeta_A^{-1}\mathbf{F}_{Ai}\,, \tag{2.2b}$$

where ζ_A and ζ_B denote friction coefficients of A and B units respectively, and the forces $\mathbf{F}_{Ai}$ and $\mathbf{F}_{Bi}$ are given by

$$\mathbf{F}_{Ai}=-\frac{\partial}{\partial\mathbf{y}_i}U=-\frac{3k_BT}{\sigma_B^2}\sum_j[\delta_{ij}(\epsilon_1+\epsilon_2)+\tfrac{1}{2}\epsilon_2A_{ij}]\times(\mathbf{y}_j-\mathbf{x}_j)\,,\quad i\neq0,N\,, \tag{2.3a}$$

$$\mathbf{F}_{Bi}=-\frac{\partial}{\partial\mathbf{x}_i}U=\frac{3k_BT}{\sigma_B^2}\sum_j[(\delta_{ij}(\epsilon_1+\epsilon_2)+\tfrac{1}{2}\epsilon_2A_{ij})\times(\mathbf{y}_j-\mathbf{x}_j)+A_{ij}\mathbf{x}_j]\,,\quad i\neq0,N\,, \tag{2.3b}$$

respectively. For the endpoints, the forces are

$$\mathbf{F}_{A0}=-\frac{3k_BT}{\sigma_B^2}[\epsilon_1(\mathbf{y}_0-\mathbf{x}_0)+\tfrac{1}{2}\epsilon_2(\mathbf{y}_1-\mathbf{x}_1)]\,, \tag{2.4a}$$

$$\mathbf{F}_{AN}=-\frac{3k_BT}{\sigma_B^2}[\epsilon_1(\mathbf{y}_N-\mathbf{x}_N)+\tfrac{1}{2}\epsilon_2(\mathbf{y}_{N-1}-\mathbf{x}_{N-1})]\,, \tag{2.4b}$$

$$\mathbf{F}_{B0}=-\mathbf{F}_{A0}+\frac{3k_BT}{\sigma_B^2}(\mathbf{x}_1-\mathbf{x}_0)\,, \tag{2.4c}$$

$$\mathbf{F}_{BN}=-\mathbf{F}_{AN}+\frac{3k_BT}{\sigma_B^2}(\mathbf{x}_{N-1}-\mathbf{x}_N)\,. \tag{2.4d}$$

The matrix $\{A_{ij}\}$ is the usual Rouse force constant matrix

$$A_{ij}=\delta_{ij+1}-2\delta_{ij}+\delta_{ij-1}\,. \tag{2.5}$$

The problem of determining the relaxation spectrum of this model is now reduced to diagonalizing a $2(N+1)\times2(N+1)$ matrix. We show in the next section and Appendix B that an exact determination of the relaxation spectrum requires the solution of three coupled transcendental equations. However, it is possible to circumvent this problem perturbatively, resulting in a series solution in powers of N^{-1}.

A second point to note is that the parameters σ_B, ϵ_1, and ϵ_2 (and perhaps other constraint parameters, e.g., those introduced in Sec. VI) may be determined rigorously for the bonded and nonbonded interatomic potentials according to the prescription given in Appendix A.

III. SOLUTION OF THE EIGENVALUE PROBLEM

In order to display the symmetry of the model, we rewrite Eqs. (2.2)–(2.4) as

$$\frac{d}{dt}\begin{bmatrix}\mathbf{x}_i(t)\\ \mathbf{y}_i(t)\end{bmatrix}=\frac{3k_BT}{\sigma_B^2\zeta_B}\begin{pmatrix}1&0\\0&\gamma\end{pmatrix}\cdot\sum_{j=0}^{N}\left[\begin{pmatrix}1-\frac{1}{2}\epsilon_2&\frac{1}{2}\epsilon_2\\ \frac{1}{2}\epsilon_2&-\frac{1}{2}\epsilon_2\end{pmatrix}A_{ij}-(\epsilon_1+\epsilon_2)\begin{pmatrix}1&-1\\-1&1\end{pmatrix}\delta_{ij}\right]\cdot\begin{bmatrix}\mathbf{x}_j(t)\\ \mathbf{y}_j(t)\end{bmatrix}\,,\quad i\neq0,N\,, \tag{3.1a}$$

$$\frac{d}{dt}\begin{bmatrix}\mathbf{x}_0(t)\\ \mathbf{y}_0(t)\end{bmatrix}=\frac{3k_BT}{\sigma_B^2\zeta_B}\begin{pmatrix}1 & 0\\ 0 & \gamma\end{pmatrix}\cdot\left\{\begin{pmatrix}1-\frac{1}{2}\epsilon_2 & \frac{1}{2}\epsilon_2\\ \frac{1}{2}\epsilon_2 & -\frac{1}{2}\epsilon_2\end{pmatrix}\cdot\begin{bmatrix}\mathbf{x}_1(t)-\mathbf{x}_0(t)\\ \mathbf{y}_1(t)-\mathbf{y}_0(t)\end{bmatrix}-(\epsilon_1+\tfrac{1}{2}\epsilon_2)\begin{pmatrix}1 & -1\\ -1 & 1\end{pmatrix}\cdot\begin{bmatrix}\mathbf{x}_0(t)\\ \mathbf{y}_0(t)\end{bmatrix}\right\}, \tag{3.1b}$$

where $\gamma\equiv\zeta_B/\zeta_A$. The equation for $i=N$ is obtained from Eq. (3.1b) by making the replacements $(0,1)\to(N,N-1)$. Equation (3.1) is clearly indicative of a chain whose repeat unit has two internal degrees of freedom. In analogy to the case of a linear diatomic chain, the model displays two sets of relaxation times corresponding to slow conformational changes in the chain and to a rapid relaxation with respect to the chain backbone. The latter process along with the AB–AB interactions provide one possible molecular mechanism for "internal viscosity."

The relaxation spectrum of Eq. (3.1) is determined by the variable transformation

$$\begin{bmatrix}\mathbf{x}_j(t)\\ \mathbf{y}_j(t)\end{bmatrix}=\sum_{k=0,\,\alpha=\pm}^{N}\Phi_{k\alpha}(j)\otimes\zeta_{k\alpha}(t)\,, \tag{3.2}$$

where $\Phi_{k\alpha}(j)$ is a 2×1 matrix. $\otimes$ denotes a direct vector product and $\zeta_{k\alpha}(t)$ is a solution of

$$\frac{d}{dt}\zeta_{k\alpha}(t)=-\frac{3k_BT}{\sigma_B^2\zeta_B}\lambda_{k\alpha}\zeta_{k\alpha}(t)\,. \tag{3.3}$$

The fundamental relaxation modes are given in terms of the set $\{\lambda_{k\alpha}\}$ in units of $3k_BT/\sigma_B^2\zeta_B$.

The exact determination of the $\{\lambda_{k\alpha}\}$ requires the solution of a fourth order difference equation with boundary conditions determined by Eq. (3.1b). In Appendix B, we show that these end point effects result in the transcendental equation

$$\cos\left(\frac{N-1}{2}\theta_{k+}\right)\cos\left(\frac{N+1}{2}\theta_{k-}\right)=\cos\left(\frac{N-1}{2}\theta_{k-}\right)\cos\left(\frac{N+1}{2}\theta_{k+}\right), \tag{3.4}$$

where θ_{k+} and θ_{k-} are also related to one another by Eq. (B5). Once the $\theta_{k\alpha}$ have been calculated, the transformation matrix $\{\Phi_{k\alpha}(j)\}$ is obtained as

$$\Phi_{k\alpha}(j)\sim\begin{bmatrix}A_{k\alpha}\\ B_{k\alpha}\end{bmatrix}[\cos(\theta_{k+}^{\alpha}j+\delta_{k+}^{\alpha})+b_{k\alpha}\cos(\theta_{k-}^{\alpha}j+\delta_{k-}^{\alpha})],$$

$$\delta_{k\pm}^{\alpha}=\text{constant}\,,\quad k=0,1,\ldots,N,\ \alpha=\pm\,.$$

We can understand the prescence of a transcendental equation for the fundamental modes as follows: In the case of a linear Rouse chain, the chain knows that it has two termination points and therefore two boundary conditions. Our model, on the other hand, has two termination side groups resulting in four boundary conditions. Consequently, the fundamental modes are determined by a transcendental equation.

For sufficiently long chains, even a chain with side groups looks like a long, thin, flexible tube with free ends. Hence, the Rouse boundary conditions should be an excellent approximation for large enough values of N. In mathematical terms, we expect

$$\Phi_{k\alpha}(j)\propto\cos\frac{\pi k}{N+1}(j+\tfrac{1}{2})\,,\ \text{for } N \text{ large enough}\,.$$

This statement is demonstrated rigorously in Appendix C. The corrections due to end effects are dealt with perturbatively and are shown to involve a series expansion in N^{-1}.

The zeroth order expression for the $\Phi_{k\alpha}(j)$ is obtained as

$$\Phi_{k\alpha}^{(0)}(j)=\sqrt{\frac{2}{N+1}}\,(1+\gamma^{-1}E_{k\alpha}^2)^{-1}\begin{bmatrix}1\\ E_{k\alpha}\end{bmatrix}\times\cos\frac{\pi k}{N+1}(j+\tfrac{1}{2})\,, \tag{3.5a}$$

where

$$E_{k\alpha}\equiv1+(\lambda_k^*-\lambda_{k\alpha}^{(0)})\Big/\left(-\frac{\epsilon_2}{2}\lambda_k^*+\epsilon_1+\epsilon_2\right), \tag{3.5b}$$

$$\lambda_k^*=4\sin^2\left[\frac{\pi k}{2(N+1)}\right]\ (\text{Rouse eigenvalue})\,, \tag{3.5c}$$

and the zeroth order eigenvalues are

$$\lambda_{k\pm}^{(0)}=\frac{1}{2}\left\{\lambda_k^*\left[1-\frac{\epsilon_2}{2}(1+\gamma)\right]+(1+\gamma)(\epsilon_1+\epsilon_2)\right\}\pm\frac{1}{2}\left(\left\{\lambda_k^*\left[1-\frac{\epsilon_2}{2}(1+\gamma)\right]+(1+\gamma)(\epsilon_1+\epsilon_2)\right\}^2-4\gamma\lambda_k^*\left(-\frac{\epsilon_2}{2}\lambda_k^*+\epsilon_1+\epsilon_2\right)\right)^{1/2}. \tag{3.6}$$

We henceforth drop the superscript "0." Expressions for the first two corrections $\{\lambda_{k\alpha}^{(1)}\}$ and $\{\lambda_{k\alpha}^{(2)}\}$ are given in Appendix C.

The eigenvalue spectrum given by Eq. (3.6) is displayed in Fig. 2 for a given set of model parameters. Note that the lower branch has a maximum at about $k^*/N\sim0.2$. Such an effect indicates that beyond k^* the slowly varying conformational motions lose energy to rapid side group motions. A similar type of behavior had previously been conjectured by Fixman and Evans[21] as a resonant energy transfer from global to local modes. However, as demonstrated by Eq. (3.6), it is possible to explain such peculiar behavior of the $\{\lambda_{k\alpha}\}$ on the basis of a very simple model of chain dynamics.

The appearance of a maximum in Fig. 2 is solely a consequence of choosing $\epsilon_2>0$. The value of the maximum, denoted by λ_{k^*-} and its location k^* are given by the following expressions:

$$\lambda_{k^*-}=\tfrac{1}{2}[2+\epsilon_2(1+\gamma)-\sqrt{8\epsilon_2}]\gamma(\epsilon_1+\epsilon_2)\left\{\left[1-\frac{\epsilon_2}{2}(1+\gamma)\right]^2+2\gamma\epsilon_2\right\}^{-1}, \tag{3.7}$$

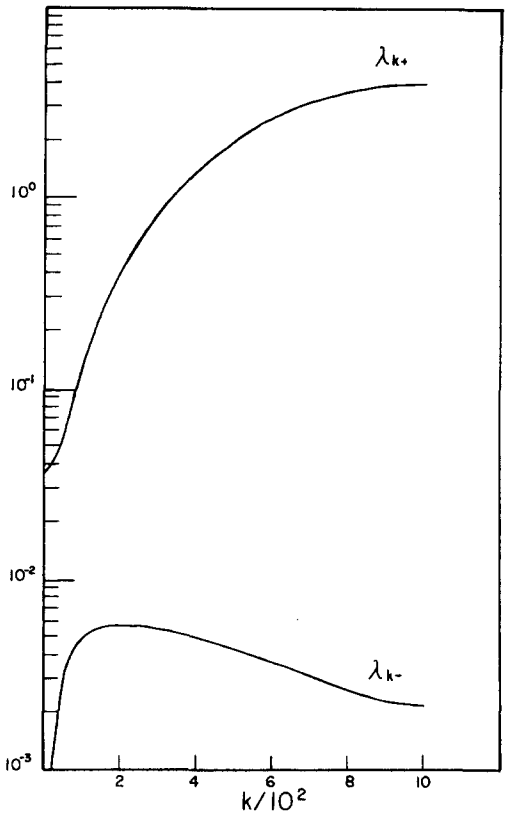

FIG. 2. Display of relaxation spectrum $\{\lambda_{k\alpha}\}$ for $N=999$, $\gamma=0.22$, $\epsilon_2=0.01$, $\epsilon_1=0.02$. The lower branch λ_{k-}, corresponding to global chain motions exhibits a maximum, λ_{k^*-} which is characteristic of calculations for syndiotactic ($\epsilon_2>0$) chains. The upper branch λ_{k+} is representative of local side group rearrangements. The presence of a gap is not associated with the first plateau in $[\eta(\omega)]$ (Fig. 4), but is related to a higher frequency second plateau region.

$$k^* = \frac{2(N+1)}{\pi} \times \sin^{-1}\frac{1}{2}\left(\frac{(\epsilon_1+\epsilon_2)\left\{\left[1-\frac{\epsilon_2}{2}(1+\gamma)\right]\left(1+\gamma-\sqrt{\frac{2}{\epsilon_2}}\right)-4\gamma\right\}}{\left[1-\frac{\epsilon_2}{2}(1+\gamma)\right]^2+2\gamma\epsilon_2}\right)^{1/2}. \tag{3.8}$$

The mode dependence of $\{E_{k\alpha}\}$ is displayed in Fig. 3. Although the $\{E_{k\alpha}\}$ do not affect the behavior of $[\eta(\omega)]$ (Sec. IV), they play significant role in dielectric relaxation (Sec. V). In particular, the dependence of E_{k-} upon k serves to select only the first few modes of λ_{k-} as contributing to the relaxation of the end-to-end vector **R**.

IV. THE INTRINSIC VISCOSITY

According to linear response theory, the intrinsic viscosity is calculated from the expression[22]

$$[\eta(\omega)] = \frac{N_A}{M\eta_0 k_B T}\int_0^\infty dt\, e^{-i\omega t}\langle J(t)J(0)\rangle\,, \tag{4.1}$$

where N_A is Avogadro's number, M is the molecular weight of the chain, and η_0 is the solvent viscosity. $\langle J(t)J(0)\rangle$ represents a two-time equilibrium correlation function of the polymer momentum flux

$$J(0) = \sum_{j=0}^{N}(F_{Bj}^{\mu}x_j^{\nu} + F_{Aj}^{\mu}y_j^{\nu})\,, \tag{4.2}$$

μ and ν denoting different Cartesian components.

Applying the transformation (3.2) to Eq. (4.2) results in an equivalent expression for $J(0)$:

$$J(0) = -\frac{3k_BT}{\sigma_B^2}\sum_{k=0,\,\alpha=\pm}^{N}\lambda_{k\alpha}\zeta_{k\alpha}^{\mu}\zeta_{k\alpha}^{\nu}\,, \tag{4.3}$$

from which the following form for the intrinsic viscosity is easily derived:

$$[\eta(\omega)] = \frac{N_A k_B T}{M\eta_0}\sum_{k,\alpha}\left[i\omega + \frac{6k_BT}{\sigma_B^2\zeta_B}\lambda_{k\alpha}\right]^{-1}(1-\delta_{k0}\delta_{\alpha-})\,. \tag{4.4}$$

It should be emphasized that Eq. (4.4) is exact for Rouse-like chains.

Plots of $[\eta(\omega)]$ [Eq. (4.4)] are given in Figs. 4 and 6 for various values of ϵ_2 and N. These curves display the following general features:

(i) The low frequency behavior is like that of a Rouse model for long enough chains.

(ii) The model displays a small plateau region which depends upon the degree of side chain motional freedom (i.e., magnitude of ϵ_2) and is independent of N for long enough chains.

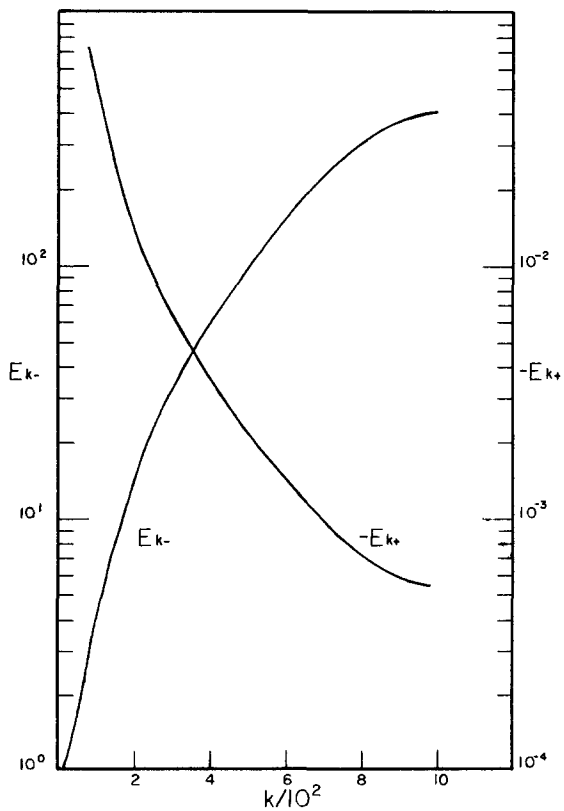

FIG. 3. Mode dependence of the side group amplitudes $\{E_{k\alpha}\}$ calculated from Eq. (3.5b) for the model parameters $N=999$, $\gamma=0.22$, $\epsilon_1=0.02$, $\epsilon_2=0.01$. E_{k-} significantly affects the behavior of the dielectric susceptibility of longitudinal dipoles (5.4) by introducing a mode cutoff beyond the first few values of λ_{k-}.

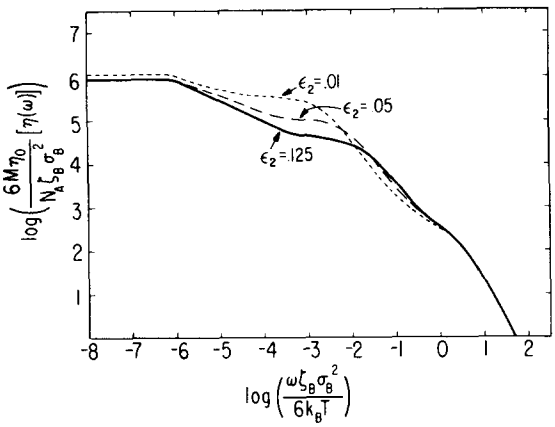

FIG. 4. Plot of $\log[\eta(\omega)]$ vs $\log\omega$ for several values of the side group interaction strength ϵ_2. Smaller values of ϵ_2 (corresponding to larger side groups) result in a larger more defined plateau region. The departure of the $\epsilon_2 = 0.01$ curve at low frequencies from the curves corresponding to $\epsilon_2 = 0.05$, 0.125 is a result of N^{-1} corrections. This vanishes for larger values of N. The model parameters chosen are $N = 999$, $\gamma = 0.22$, $\epsilon_1 = 2\epsilon_2$.

(iii) The model indicates the beginning of a second plateau region at even higher frequencies corresponding roughly to the gap $\lambda_{N+} - \lambda_{k^*-}$, λ_{k^*-} being given by Eq. (3.7). (The gap region is denoted by vertical bars on the abscissa.)

(iv) For short chains ($N \leq 10^2$ for the parameters chosen), the plateau region vanishes. This disappearance occurs when N decreases to the point where $[\eta(0)]$ becomes equal to $[\eta]_\infty$. Figure 7 suggests that $\sim 10^2$ units are involved in producing the plateau viscosity $[\eta]_\infty$. The low frequency behavior of $[\eta(\omega)]$ is strongly affected by the presence of the side groups as the intrinsic viscosity becomes molecular weight dependent for short enough chains, thereby departing from a simple Rouse result in this limit. This behavior is displayed in Figs. 6 and 7, where the dashed lines give the simple Rouse results with $\zeta_{eff} = \zeta_A + \zeta_B$, while the solid curves present the model predictions. This small N departure from Rouse model behavior will persist when hydrodynamic interactions are included. These calculations are in general accord with the experimentally observed lack of pure power law variation of $[\eta(0)]$ with N for low molecular weights.[5]

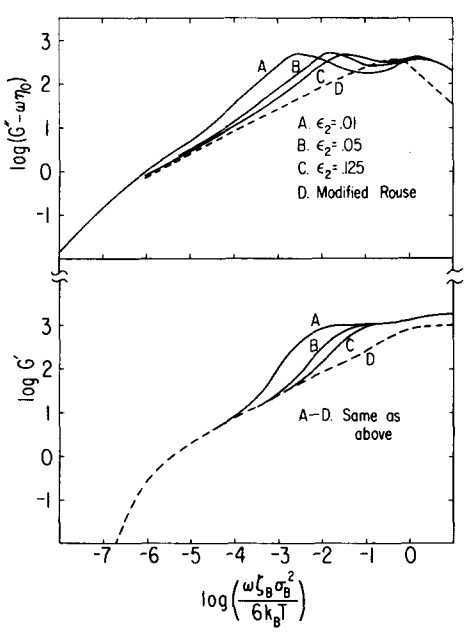

FIG. 5. The complex elastic moduli as a function of frequency given for the same model parameters as in Fig. 4. The dashed curves represent the moduli for an effective Rouse model whose parameters are given by $\zeta_{eff} = \zeta_A + \zeta_B$, $\sigma_{eff} = \sigma_B$, whereas the solid curves correspond to the model with side group interactions. The loss curve (a) displays two regions of first power law dependence on ω. The storage modulus [curve (b)] displays on increasing behavior at high frequencies, indicating a trend which is in agreement with experiments to date, as opposed to a flattening out which had previously been thought to occur.[26]

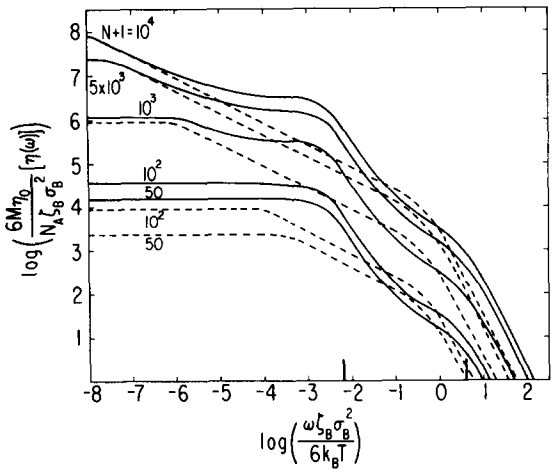

FIG. 6. Plot of $\log[\eta(\omega)]$ vs $\log\omega$ for several values of N and $\gamma = 0.22$, $\epsilon_2 = 0.01$, $\epsilon_1 = 0.02$. The solid curves represent calculations based on the model, and the dashed curves are obtained for the corresponding effective Rouse model. The vertical lines on the abscissa correspond to the gap region, $\lambda_{N+} - \lambda_{k^*-}$, between the upper branch and the lower branch maximum, λ_{k^*-}, indicating that the first plateau is not due to the presence of a gap in the relaxation spectrum. The gap instead corresponds to a higher frequency, second plateau. The first plateau $[\eta]_\infty$ is also seen to decrease in magnitude and to eventually vanish as N decreases. This occurs as a consequence of the comparability of the relaxation rates of "local" and global chain motions. The model behavior indicated for $N+1 = 50$, 100, as compared to the corresponding effective Rouse curves, demonstrates that short chain behavior is inadequately described as a Rouse chain. Notice here the difference in the molecular weight dependence of $[\eta(0)]$ between the model and the Rouse case for small N. This departure is emphasized in Fig. 7(a).

Figure 5 displays both components of the complex modulus $G(\omega) \equiv i\omega\eta_0\{1 + [\eta(\omega)]\}$ for the same parameters as in Fig. 4. Several features of these curves are worth noting: (i) The loss modulus $G'' - i\omega\eta_0$ behavior indicates a first power law dependence on frequency for frequencies below and just beyond the plateau region in agreement with experiment. (ii) Experimental data for the storage modulus G' indicate an upward trend just beyond the plateau region. The curve for $G'(\omega)$ displays such a behavior at a frequency $\omega \sim 10^{-4}(6k_BT/\sigma_B^2\zeta_B)$ for the parameters chosen. However, contrary to experiment, it has been believed[26] that $G'(\omega)$ should flatten in

this frequency regime. Thus, the model demonstrates that $G'(\omega)$ flattens out at a much higher frequency than heretofore believed, in agreement with experiment.

In order to understand some of these qualitative features quantitatively, it is necessary to further develop Eq. (4.4). Performing the α summation recognizing that quantities like $\lambda_{k+}\lambda_{k-}$ and $\lambda_{k+}+\lambda_{k-}$ involve simple polynomials in λ_k^*, and regrouping pairs of $\alpha=\pm$ terms for each k in Eq. (4.4) demonstrates that Eq. (4.4) exhibits the structure

$$I=\sum_{k=1}^{N} P_n(\lambda_k^*)/L_m(\lambda_k^*)\ , \tag{4.5}$$

where P_n and L_m are polynomials of degree n and m, respectively, and $m>n$. A closed analytic form for I is derived in Appendix D. This result is then applied to Eq. (4.4) in Appendix E to produce the closed analytic expression for $[\eta(\omega)]$:

$$[\eta(\omega)]=-\frac{N_A\zeta_B\sigma_B^2}{6\gamma\epsilon_2 M\eta_0}\sum_{\alpha=\pm}\frac{2i\bar{\omega}+\eta_\alpha(\bar{\omega})\left[1-\frac{\epsilon_2}{2}(1+\gamma)\right]+(1+\gamma)(\epsilon_1+\epsilon_2)}{\eta_\alpha(\bar{\omega})-\eta_{-\alpha}(\bar{\omega})}$$
$$\times\frac{[1-\frac{1}{2}\eta_\alpha(\bar{\omega})]\eta_\alpha^{-1/2}(\bar{\omega})[1-\frac{1}{4}\eta_\alpha(\bar{\omega})]^{-1/2}-(N+1)\cot\{2(N+1)\sin^{-1}[\frac{1}{2}\eta_\alpha^{1/2}(\bar{\omega})]\}}{\eta_\alpha^{1/2}(\bar{\omega})[1-\frac{1}{4}\eta_\alpha(\bar{\omega})]^{1/2}}+\frac{N_A\zeta_B\sigma_B^2}{6\eta_0 M[i\omega+(1+\gamma)(\epsilon_1+\epsilon_2)]}\ , \tag{4.6}$$

where $\eta_\pm(\bar{\omega})$ are defined by

$$\eta_\pm(\bar{\omega})\equiv\frac{1}{\gamma\epsilon_2}\left\{\gamma(\epsilon_1+\epsilon_2)+i\bar{\omega}\left[1-\frac{\epsilon_2}{2}(1+\gamma)\right]\right\}$$
$$\pm\frac{1}{\epsilon_2\gamma}\left(\left\{\gamma(\epsilon_1+\epsilon_2)+i\bar{\omega}\left[1-\frac{\epsilon_2}{2}(1+\gamma)\right]\right\}^2+2\epsilon_2\gamma[-\bar{\omega}^2+i\bar{\omega}(1+\gamma)(\epsilon_1+\epsilon_2)]\right)^{1/2}\ , \tag{4.7}$$

and the dimensionless frequency is

$$\bar{\omega}\equiv\omega\zeta_B\sigma_B^2/6k_BT\ . \tag{4.8}$$

Taking the limit in which $\bar{\omega}\to 0$ in Eq. (4.6) yields two terms corresponding to $\alpha=\pm$,

$$[\eta(0)]=\frac{N_A\zeta_B\sigma_B^2}{M\eta_0}\left[\frac{1+\gamma}{36\gamma}(N^2+2N)\right.$$
$$\left.+\frac{1}{6\gamma}\left(\frac{(N+1)\coth\left\{2(N+1)\sinh^{-1}\left[\frac{2}{\epsilon_2}(\epsilon_1+\epsilon_2)\right]\right\}+\epsilon_1(\epsilon_1^2-\epsilon_2^2)^{-1/2}}{(\epsilon_1^2-\epsilon_2^2)^{1/2}}\right)+\tfrac{1}{6}(1+\gamma)^{-1}(\epsilon_1+\epsilon_2)^{-1}\right]\ . \tag{4.9}$$

In the limit as $N\to\infty$, $[\eta(0)]$ is dominated by the first term in Eq. (4.9):

$$[\eta(0)]=\frac{N_A\sigma_B^2(\zeta_A+\zeta_B)}{M\eta_0}\frac{N^2}{36}[1+O(N^{-1})]\ . \tag{4.10}$$

Therefore, at zero frequency and for long chains, the model behaves like a Rouse chain with an effective friction coefficient per segment $\zeta_{eff}=\zeta_A+\zeta_B$, which is the sum of backbone and side group friction coefficients, and with an effective mean square end-to-end distance $\langle\mathbf{R}_{eff}^2\rangle=N\sigma_B^2$. This physically transparent decomposition is further emphasized by noting that the small frequency behavior of $[\eta(\omega)]$ is primarily determined by λ_{k-}, in particular the small k/N or λ_k^* terms. However, from Eq. (3.6), we find that

$$\lambda_{k-}\simeq(\zeta_A+\zeta_B)^{-1}\zeta_B\lambda_k^*\ ,\quad \text{for } \lambda_k^* \text{ small}\ . \tag{4.11}$$

Hence, at low frequencies, Eq. (4.4) is approximated by

$$[\eta(\omega)]\simeq\frac{N_Ak_BT}{M\eta_0}\sum_{k=1}^{N}\left[i\omega+\frac{6k_BT}{\sigma_B^2}(\zeta_A+\zeta_B)^{-1}\lambda_k^*\right]^{-1}\ , \tag{4.12}$$

which is the intrinsic viscosity for a Rouse chain with the aforementioned parameters.

At frequencies which coincide with the plateau region depicted in Figs. 4 and 6, the $\alpha=-$ term in Eq. (4.6) is falling off roughly as $\omega^{-1/2}$. The $\alpha=+$ term is still well approximated by the second term in Eq. (4.9). We, therefore, have an approximate expression for the plateau value $[\eta]_\infty$ given by

$$[\eta]_\infty\simeq\frac{N_A\zeta_B\sigma_B^2}{6\gamma M\eta_0}\left(\frac{(N+1)\coth\left\{2(N+1)\sinh^{-1}\left[\frac{2}{\epsilon_2}(\epsilon_1+\epsilon_2)\right]\right\}+(\epsilon_1^2-\epsilon_2^2)^{-1/2}\epsilon_1}{(\epsilon_1^2-\epsilon_2^2)^{1/2}}\right)$$
$$+\frac{N_A\zeta_B\sigma_B^2}{6M\eta_0(1+\gamma)(\epsilon_1+\epsilon_2)}-\frac{N_A\zeta_B\sigma_B^2N}{6\gamma M\eta_0(\epsilon_1^2-\epsilon_2^2)^{1/2}}\ \text{as}\ N\to\infty\ . \tag{4.13}$$

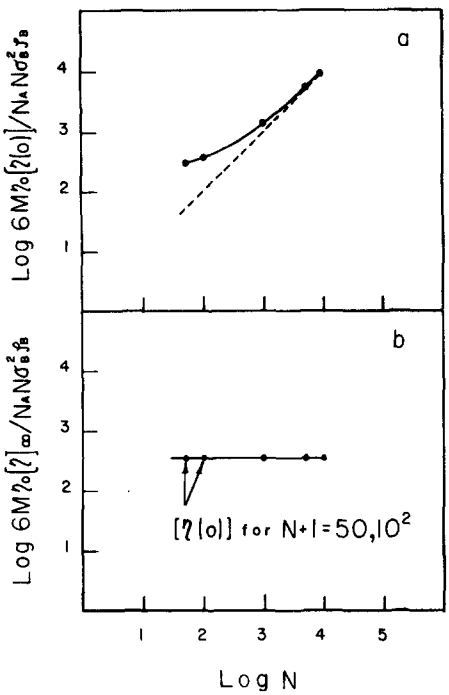

FIG. 7. Variation of $\log[\eta(0)]$ [curve (a)] and $\log[\eta]_\infty$ [curve (b)] as a function of $\log N$ (values taken from Fig. 6). The dashed curve in figure a corresponds to $[\eta(0)]$ for the effective Rouse model. The deviation from Rouse chain behavior for short chains is quite evident. In the lower curve (b), $[\eta]_\infty$'s are chosen for $N+1=10^3$, 5×10^3, 10^4. The points corresponding to $N+1=50$, 10^2 are $[\eta(0)]$ values taken from curve (a), indicating that $\sim10^2$ units are involved in producing $[\eta]_\infty$.

It is evident from Eq. (4.13) that $[\eta]_\infty$ is independent of molecular weight for long enough chains. Furthermore, the plateau value is independent of whether the chain is isotactic ($\epsilon_2<0$) or syndiotactic ($\epsilon_2>0$) provided that $|\epsilon_2|<\epsilon_1$. We have checked the former numerically for the parameters chosen in Fig. 6 with $\epsilon_2=-0.01$ and found $[\eta]_\infty$ to be unaltered due to a change in sign of ϵ_2. The magnitude of γ does not affect the height of $[\eta]_\infty$ relative to $[\eta(0)]$ significantly. However, the second plateau, discussed earlier, becomes more pronounced as γ decreases.

For shorter chains ($N\lesssim10^2$ for the parameters chosen), the $\alpha=+$ term begins to dominate in (4.6) thereby washing out the first plateau region. This behavior is depicted in Figs. 6 and 7.

V. DIELECTRIC RELAXATION

A. Longitudinal dipole relaxation

The expression for the dielectric susceptibility given by linear response theory is[27]

$$\chi(\omega)=-\frac{1}{k_BT}\int_0^\infty dt\,e^{-i\omega t}\left\langle\mu(0)\frac{d}{dt}\mu(t)\right\rangle\,, \tag{5.1}$$

where μ is the total dipole moment for a chain in a given direction, say the ν direction. For dipole moments situated along the chain backbone, μ is given by

$$\mu=\mu_B\sum_{i=0}^{N}(x_{i+1}^\nu-x_i^\nu) \tag{5.2a}$$

$$\equiv\mu_BR^\nu\,, \tag{5.2b}$$

where μ_B is the dipole per unit length for the chain backbone, and R^ν is the ν component of the end-to-end vector. Equation (5.1) is now written as

$$\chi_{BB}(\omega)=-\frac{\mu_B^2}{k_BT}\int_0^\infty dt\,e^{-i\omega t}\left\langle R^\nu(0)\frac{d}{dt}R^\nu(t)\right\rangle\,. \tag{5.3}$$

Applying the transformation given by Eqs. (3.2), (3.5), and (3.6) to Eq. (5.3) results in the expression

$$\chi_{BB}(\omega)=\frac{8\mu_B^2}{\zeta_B(N+1)}\sum_{k\ \text{odd},\,\alpha}\cos^2\left[\frac{\pi k}{2(N+1)}\right]\times(1+E_{k\alpha}^2\gamma^{-1})^{-1}\left(i\omega+\frac{3k_BT}{\sigma_B^2\zeta_B}\lambda_{k\alpha}\right)^{-1}\,. \tag{5.4}$$

Again, at very low frequencies, the most significant contribution to $\chi_{BB}(\omega)$ comes from the first few (Rouse-like) modes of the minus branch. This selectivity is due both to the behavior of λ_{k-} for small k and the rapidly increasing behavior of E_{k-} beyond the first several "Rouse-like" modes. Thus, we have the approximate expression

$$\chi_{BB}(\omega)\simeq\frac{8\mu_B^2}{N+1}(\zeta_A+\zeta_B)^{-1}\sum_{\substack{k\ \text{odd}\\ k<k_{max}}}\cos^2\left[\frac{\pi k}{2(N+1)}\right]\times\left[i\omega+\frac{3k_BT}{\sigma_B^2}(\zeta_A+\zeta_B)^{-1}\lambda_k^*\right]^{-1}\,, \tag{5.5}$$

where E_{k-} [Eq. (3.5b)] is well approximated by unity for the first several values of k (i.e., perhaps the first 10 modes). Equation (5.5) is the usual result for the dielectric susceptibility of a Rouse chain provided that the cutoff k_{max}, can be extended to N. Since the first few Rouse modes dominate, this extension can be introduced without too much difficulty. The behavior of Eqs. (5.4) and (5.5), with $k_{max}=N$ in the latter, is compared in Figs. 8 and 9. A closed analytic expression for $\chi_{BB}(\omega)$ is given in Appendix E.

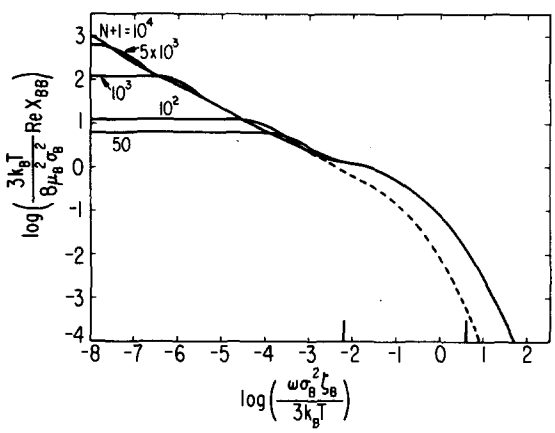

FIG. 8. Variation of the dielectric storage for longitudinal dipoles as a function of w for several values of N and $\gamma=0.22$, $\epsilon_1=0.02$, $\epsilon_2=0.01$. The dashed curve represents the effective Rouse model calculation, and the vertical bars on the abscissa again correspond to the gap region in the relaxation spectrum. The model is seen to correspond to the effective Rouse model except for frequencies in and above the gap region.

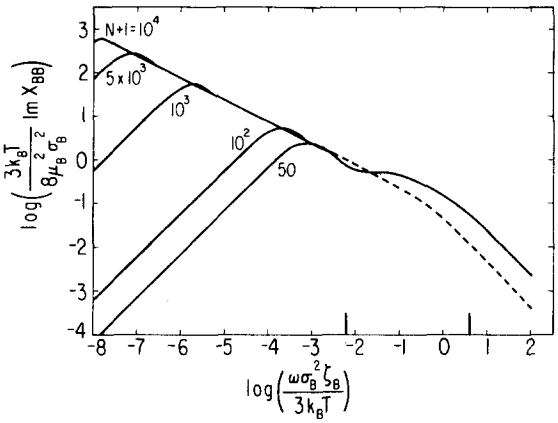

FIG. 9. The dielectric loss for longitudinal dipoles as a function of ω for the same parameters as in Fig. 8. The relaxation of longitudinal dipoles is again well represented in terms of Rouse model dynamics except at higher frequencies where the second branch becomes important.

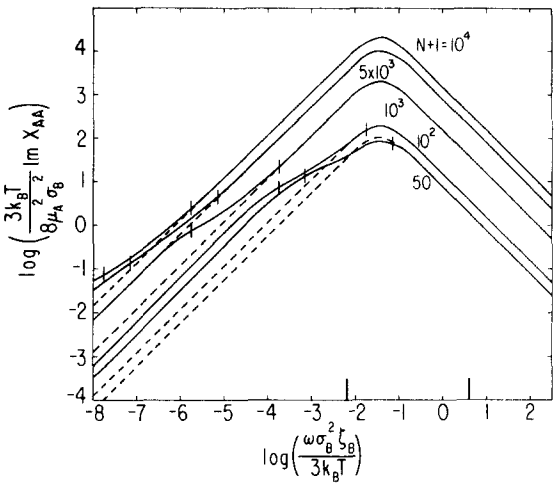

FIG. 11. Dielectric loss for perpendicular dipole relaxation as a function of frequency for the same parameters as in Fig. 10. The dashed curves represent the shifted Rouse model calculations. Both models are seen to be in agreement for frequencies in and above the gap region (vertical bars on abscissa) for long enough chains ($N \geq 10^3$). Deviations in the two models occur at lower frequencies corresponding roughly to the first ten modes in λ_{k-}. (Vertical bars on curves designate the relaxation frequencies of the first and tenth modes.) This effect is particularly significant for short chains ($N \leq 10^2$) and, as a result, can shift the frequency of maximum loss to lower values.

B. Perpendicular dipole relaxation

Let μ_A denote the dipole moment per unit length along a side group. Then Eq. (5.1) becomes

$$\chi_{AA}(\omega) = -\frac{\mu_A^2}{k_B T}\int_0^\infty dt\, e^{-i\omega t}\left\langle S(0)\frac{d}{dt}S(t)\right\rangle , \tag{5.6}$$

where

$$\mu = \mu_A \sum_{i=0}^{N}(y_i^\nu - x_i^\nu) \equiv \mu_A S \tag{5.7}$$

is the total perpendicular dipole moment.

It is necessary to proceed cautiously in the evaluation of $\chi_{AA}(\omega)$. The approximate transformation (3.5) and (3.6) are not applicable to the total side group dipole moment $\mu_A S$ by virtue of the sensitivity in the evaluation of S to the approximate treatment of end effects. This difficulty is circumvented, however, by modifying the Rouse boundary conditions to that of a free side group on each end of the chain plus end effect corrections which are treated perturbatively. This problem is considered in detail in the second part of Appendix C. The appropriate transformation for S is given by Eq. (C25), and therefore $\chi_{AA}(\omega)$ is found to be equal to

$$\chi_{AA}(\omega) = \frac{2\mu_A^2}{\zeta_B}\frac{1}{N+1}\sum_{k\,\mathrm{odd},\alpha}\cot^2\left[\frac{\pi k}{2(N+1)}\right] \times \frac{(E_{k\alpha}-1)^2}{(1+\gamma^{-1}E_{k\alpha}^2)(i\omega + 3k_B T\lambda_{k\alpha}/\sigma_B^2\zeta_B)} , \tag{5.8}$$

where the replacement $N+2 \to N+1$ is made. Corrections due to end effects are again negligible for N large.

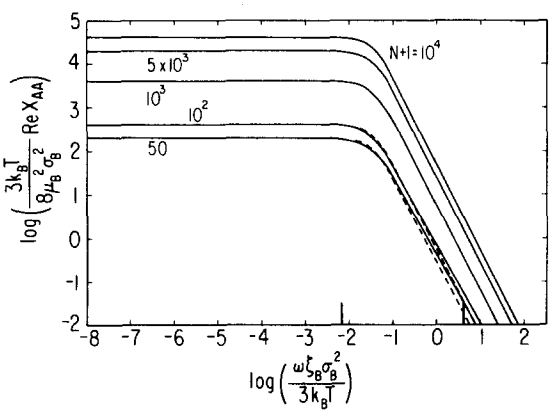

FIG. 10. Dielectric storage for perpendicular dipoles relaxation as a function of frequency for several values of N and for $\gamma = 0.22$, $\epsilon_1 = 0.02$, $\epsilon_2 = 0.01$. Vertical bars on the abscissa, on before, correspond to the gap region in the relaxation spectrum. The dashed curves represent the shifted Rouse model calculations taken from Eqs. (5.11)–(5.13) with $\theta = 4/\gamma$, $\zeta_{eff} = \zeta_A/4$, $\sigma_{eff}^2 = \sigma_B^2/(\epsilon_1+\epsilon_2)$.

The qualitative behavior of $\chi_{AA}(\omega)$ is depicted in Figs. 10 and 11 for several values of N. The dashed curves represent a comparison to the shifted Rouse model discussed below. The location of the gap region, designated by $\lambda_{N+} - \lambda_{k^*-}$, is indicated by vertical bars. The location of the λ_{1-} and λ_{10-} modes are similarly indicated on the loss curves. These figures display an independence upon N in the dielectric storage, whereas the loss curves indicate a small N dependence for $N \geq 10^3$ (for values of ϵ_1, ϵ_2, and γ chosen) which becomes more pronounced for $N < 10^3$. The large frequencies at which relaxation occurs shows that the $\{\lambda_{k+}\}$ (see vertical bars on frequency scale) play the significant role in the behavior of the chain side groups. The small molecular weight dependence in the loss curves is associated with the $\{\lambda_{k-}\}$ (see vertical bars on loss curves) or global motions of the chain, which is in accord with the suggestion of Stockmayer and co-workers regarding the interpretation of the experimental data.[13] A closed analytic expression for $\chi_{AA}(\omega)$ is given in Appendix E. Two limiting values of Eq. (E12) are of interest:

$$\lim_{\omega\to 0}\chi_{AA}(\omega)\to\frac{N}{3k_BT}\frac{\mu_A^2\sigma_B^2}{\epsilon_1+\epsilon_2}\,,\quad N\text{ large}\,, \tag{5.9a}$$

$$\lim_{\omega\to\infty}\mathrm{Re}\,\chi_{AA}(\omega)\to\frac{N}{3k_BT}\frac{\mu_A^2\sigma_B^2}{\bar{\bar{\omega}}^2}(1+\gamma)^2(\epsilon_1+\epsilon_2)\,,\quad N\text{ large}\,, \tag{5.9b}$$

where

$$\bar{\bar{\omega}}\equiv\omega\zeta_B\sigma_B^2/3k_BT\,. \tag{5.10}$$

Consider a Rouse chain whose beads are designated by the vectors $\{\mathbf{z}_i\}_{i=0,1,\ldots,N}$. The total perpendicular dipole moment for such a chain is customarily taken as proportional to

$$D\equiv\sum_{j=0}^{N-1}(-1)^j(z_{j+1}^\nu-z_j^\nu)\,. \tag{5.11}$$

If we can assume that the strength of each dipole is given by μ_A, then the dielectric susceptibility derived from Eq. (5.11) is given by

$$\chi_D(\omega)=-\frac{\mu_A^2}{k_BT}\int_0^\infty dt\,e^{-i\omega t}\left\langle D(0)\frac{d}{dt}D(t)\right\rangle \tag{5.12a}$$

$$=\frac{2\mu_A^2}{k_BT}\frac{1}{N+1}\sum_{\substack{k=1\\ k\text{ odd}}}^{N}\tan^2\left[\frac{\pi k}{2(N+1)}\right]$$

$$\times\lambda_k^*(i\omega+3k_BT\lambda_k^*/\sigma_{eff}^2\zeta_{eff})^{-1}\,, \tag{5.12b}$$

where σ_{eff} and ζ_{eff} denote the effective Kuhn length and friction coefficient, respectively. According to Dubois-Violette and co-workers,[14,15] and Stockmayer *et al.*,[16] in order to reproduce experimental data, Eq. (5.12b) should be modified so that

$$\chi_D(\omega)=\frac{2\mu_A^2}{k_BT}\frac{1}{N+1}\sum_{k\text{ odd}}\tan^2\left[\frac{\pi k}{2(N+1)}\right](\lambda_k^*+\theta)$$

$$\times\left[i\omega+\frac{3k_BT}{\sigma_{eff}^2\zeta_{eff}}(\lambda_k^*+\theta)\right]^{-1}\,, \tag{5.13}$$

where the new parameter θ is supposed to represent the presence of local barriers to relaxation neglected by the Rouse model.

A comparison of $\chi_{AA}(\omega)$ to the phenomenological form $\chi_D(\omega)$ [Eq. (5.13)] is facilitated by observing the zero frequency and large frequency behavior of each. The limiting behavior of Eq. (5.13) corresponding to Eq. (5.9) is

$$\lim_{\omega\to 0}\chi_D(\omega)=\frac{N}{3k_BT}\mu_A^2\sigma_{eff}^2\,,\quad N\text{ large}\,, \tag{5.14a}$$

$$\lim_{\omega\to\infty}\mathrm{Re}\,\chi_D(\omega)=\frac{N}{3k_BT}\frac{\mu_A^2\sigma_{eff}^2}{\omega^2}\left(\frac{3k_BT}{\sigma_{eff}^2\zeta_{eff}}\right)^2(4+\theta)^2\,, \tag{5.14b}$$

from which the following identifications are made:

$$\sigma_{eff}^2=\sigma_B^2/(\epsilon_1+\epsilon_2)\,, \tag{5.15}$$

$$(4+\theta)/\zeta_{eff}=(1+\gamma)/\zeta_B\,. \tag{5.16}$$

It is clear from Eq. (5.16) that there is a degree of arbitrariness in the comparison of the two models since there are two equations for the three unknowns σ_{eff}, ζ_{eff}, and θ. Equation (5.15) suggests, however, that side group motions are dominant in the behavior of $\chi_{AA}(\omega)$. Therefore, we expect $\zeta_{eff}\sim\zeta_A$. With this in mind, $\chi_D(\omega)$ is displayed in Figs. 11 and 12 with the selections

$$\theta=4/\gamma\,,\quad \zeta_{eff}=\zeta_A/4\,, \tag{5.17}$$

and σ_{eff} being given by Eq. (5.15). This shifted Rouse ansatz gives a good representation of our model for the real part of $\chi_{AA}(\omega)$ (storage) and deviates from $\mathrm{Im}\,\chi_{AA}(\omega)$ at low frequencies corresponding to the vertical markers on the loss curves. These deviations are solely due to the effect of global chain motions on $\chi_{AA}(\omega)$. The region of matching between the two models are therefore attributed to the high frequency $\{\lambda_{k+}\}$ relaxation which is evident from the regions of overlap in the two models (vertical bars on the frequency scale).

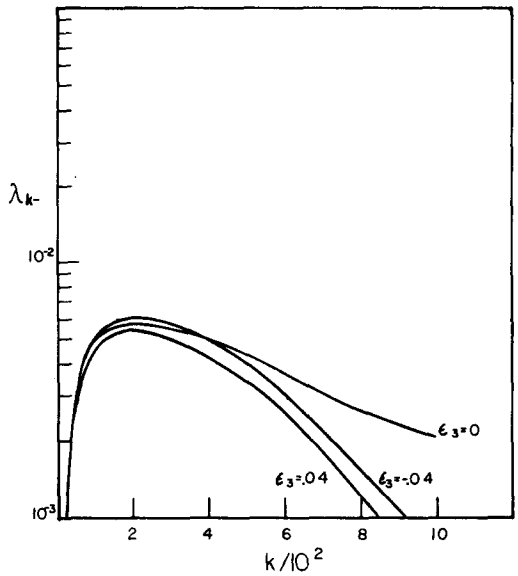

FIG. 12. Mode dependence of λ_{k-} for several values of the additional ABB bond angle constraint ϵ_3 and $\gamma=0.22$, $\epsilon_1=0.02$, $\epsilon_2=0.01$, $N=999$. Nonzero values of the constraint have the effect of further depressing (in magnitude) the large k behavior of λ_{k-}. No significant change is noted in the behavior of λ_{k+} for different values of ϵ_3.

VI. ADDITIONAL CONSTRAINTS

The interactions considered thus far have only accounted for chain connectivity and relative orientation of neighboring side groups. Additional constraints within the model, which involve interactions between next nearest neighbor segments, etc., are obtained from the generalized equation of motion [Eq. (A16)]. One such constraint, considered below, specifies the orientation of an AB segment relative to its neighboring BB backbone bond vector. We therefore add the term

$$\frac{3k_BT}{2\sigma_B^2}\epsilon_3\Big\{(\mathbf{y}_0-\mathbf{x}_0)\cdot(\mathbf{x}_1-\mathbf{x}_0)+\sum_{i=1}^{N-1}[(\mathbf{y}_i-\mathbf{x}_i)\cdot(\mathbf{x}_{i+1}-\mathbf{x}_i)$$

$$-(\mathbf{y}_i-\mathbf{x}_i)\cdot(\mathbf{x}_i-\mathbf{x}_{i-1})]-(\mathbf{y}_N-\mathbf{x}_N)\cdot(\mathbf{x}_N-\mathbf{x}_{N-1})\Big\} \tag{6.1}$$

to Eq. (2.1). Equation (6.1) has the effect of setting up a preferred local BB–AB–BB geometry. For positive values of ϵ_3, the preferred geometry of the chain is similar to that depicted in Fig. 1, and the term (6.1) tends

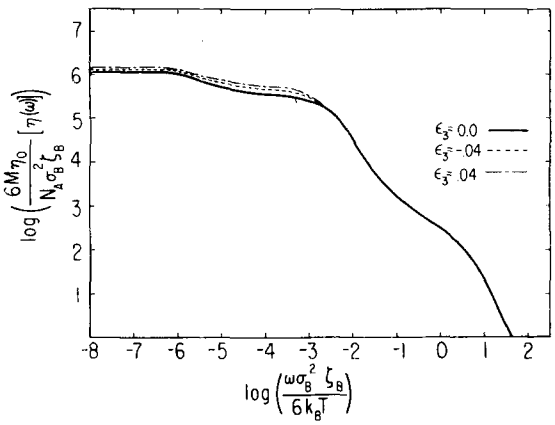

FIG. 13. Log$[\eta(\omega)]$ vs logω for the same parameters as Fig. 12. The additional constraint gives a somewhat more pronounced plateau $[\eta]_\infty$ because ABB bond angle constraints enhance the degree of hindered rotational motion. Differences in the low frequency behavior are due to N^{-1} corrections.

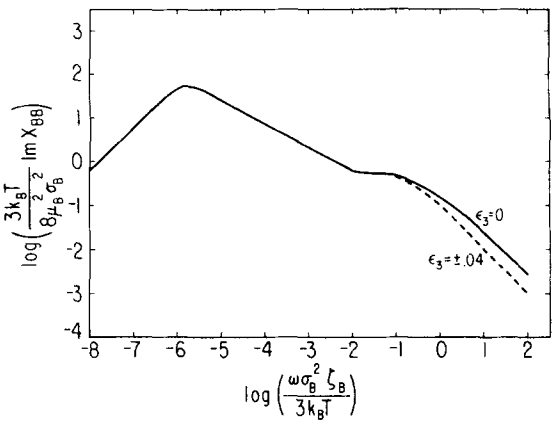

FIG. 15. Same as Fig. 14 for dielectric loss. No significant changes are found for perpendicular dipole relaxation.

to keep the A_i–B_i bond vectors in the plan perpendicular to the line joining the B_{i+1} and B_{i-1} backbone units. This in turn enhances the effects of A_iB_i–$A_{i\pm1}B_{i\pm1}$ bond interactions because of the resultant increased restriction on side group motions.

The eigenvalue spectrum is determined using the same considerations that resulted in Eq. (3.6). As a result, we find the $\{\lambda_{k\alpha}\}$ are given by

$$\lambda_{k\pm}=\frac{1}{2}\left\{\left[1+\epsilon_3-\frac{\epsilon_2}{2}(1+\gamma)\right]\lambda_k^*+(1+\gamma)(\epsilon_1+\epsilon_2)\right\}$$
$$\pm\frac{1}{2}\left(\left\{\left[1+\epsilon_3-\frac{\epsilon_2}{2}(1+\gamma)\lambda_k^*\right]+(1+\gamma)(\epsilon_1+\epsilon_2)\right\}^2\right.$$
$$\left.-4\gamma\lambda_k^*\left[(1-\epsilon_3)\left(-\frac{\epsilon_2}{2}\lambda_k^*+\epsilon_1+\epsilon_2\right)-\epsilon_3^2\lambda_k^*\right]\right)^{1/2}. \quad (6.2)$$

Mathematical considerations indicated that there exists only a small range of values of ϵ_3 for which the $\{\lambda_{k\alpha}\}$ are in the physical positive semidefinite regime. Numerical comparisons of the $\{\lambda_{k\alpha}\}$, intrinsic viscosity, and dielectric dispersion are given for two nonzero values of ϵ_3 in Figs. 11–15 for fixed values of N, γ, ϵ_1, and ϵ_2. These curves suggest that the somewhat more depressed λ_{k-} for $\epsilon_3\neq0$ can produce a more pronounced plateau in $[\eta(\omega)]$ but does not significantly affect the dielectric behavior. The approximate limitation on $|\epsilon_3|$ for the values of ϵ_1, ϵ_2, γ, and N chosen is $|\epsilon_3|<0.05$.

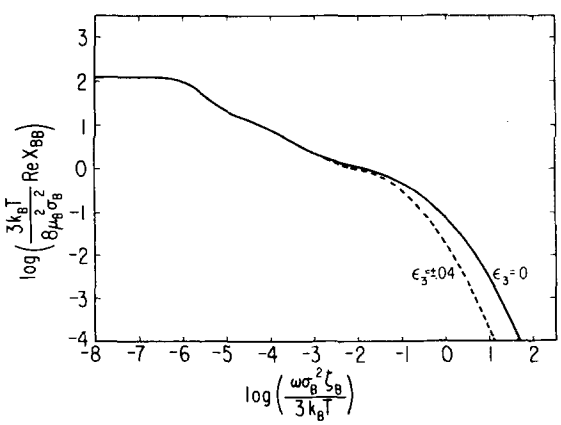

FIG. 14. The effect of the additional constraint upon the dielectric storage for longitudinal dipoles using the parameters given in Fig. 12. The dashed curve corresponds to $\epsilon_3=\pm0.04$ and the solid curve to $\epsilon_3=0.0$.

VII. CONCLUSION

We present a model of polymer chain dynamics in which the effects of side group interactions are explicitly treated. Calculations for the relaxation spectrum $\{\lambda_{k\alpha}\}$, intrinsic viscosity $[\eta(\omega)]$, and dielectric dispersion for both longitudinal and perpendicular dipole moments χ_{BB} and χ_{AA}, respectively, are presented in the free draining limit. Closed analytic expressions are given for all correlation functions of interest. The results of these calculations may be summarized as follows:

(i) The relaxation spectrum $\{\lambda_{k\alpha}\}$ displays two branches. The lower branch has a maximum for $\epsilon_2>0$ at a mode number k^* [Eq. (3.8)] beyond which it is depressed.

(ii) The low frequency behavior of the intrinsic viscosity $[\eta(\omega)]$ is well represented by an effective Rouse model for long enough chains whose parameters are given by

$$\sigma_{eff}=\sigma_B\,, \quad (7.1a)$$

$$\zeta_{eff}=\zeta_B+\zeta_A\,, \quad \text{for } \epsilon_3=0\,. \quad (7.1b)$$

(iii) At higher frequencies, the model displays a plateau $[\eta]_\infty$ which is independent of molecular weight for long enough chains and is correlated to the degree of side group motional freedom in agreement with the experiments of Ferry, Schrag, and co-workers.[4,5] The value of $[\eta]_\infty$ is independent of whether the side group interactions favor isotactic or syndiotactic allignment. If the friction coefficients ζ_A and ζ_B are taken to be proportional to solvent viscosity η_0, then the derived expression for $[\eta]_\infty$ [Eq. (4.13)] is independent of η_0. The presence of $[\eta]_\infty$ in our model is *not* a consequence of the gap in the relaxation frequency spectrum.

(iv) The low frequency behavior of our model for

short enough chains still contains effects due to the presence of the side groups which cannot be adequately represented by a Rouse model. Hence, our model displays a departure of the first power law dependence of $[\eta(0)]$ on N for small N. This result must persist when hydrodynamic interactions are incorporated, and it is in agreement with experimental observations.

(v) The dielectric relaxation of longitudinal dipoles is characterized by the same effective Rouse model given in (ii) apart from high frequency corrections due to the upper branch in the relaxation spectrum.

(vi) The relaxation of perpendicular dipoles is described by attaching a dipole moment to each side group. The corresponding correlation function $\chi_{AA}(\omega)$ decays at a frequency which is independent of molecular weight (for N large enough), indicating that local effects are of major importance. For short chains, however, global chain motions (e.g., overall rotation and the other few slowest relaxation modes) significantly affect the behavior of the dielectric loss. $\chi_{AA}(\omega)$ corresponds well to the phenomenological model proposed by Dubois-Violette and co-workers, and Stockmayer *et al.*, to fit their experimental data. This relationship is established, in part, by observing the limiting behaviors of $\chi_{AA}(\omega)$ [Eq. (5.8)] and $\chi_D(\omega)$ [Eq. (5.13)]. Although such a procedure is neither fundamental or unique, the comparisons appear to agree quite well for high frequencies.

(vii) The effect of an additional constraint, which sets up a more realistic local geometry, provides some qualitative improvement in the behavior of the correlation functions of interest. However, the essential physics is contained in the free energy given by Eq. (2.1).

The parameters appearing in the model (ϵ_1, ϵ_2, ϵ_3, etc.) can be calculated from realistic interatomic potentials. The prescription for performing these calculations is given in terms of a generalized force constant matrix obtained in Appendix A.

A number of problems are still left unresolved. Equation (4.13) indicates that $[\eta]_\infty$ is independent of η_0 which is probably true only in the limit of large solvent viscosity. The work of Edwards and Goodyear[28] indicates that the surpressed true potentials (and by extension of their arguments, the surpressed degrees of freedom) provide a solvent viscosity independent contribution to internal chain friction forces. A particular example has been provided by de Gennes,[29] and our discussions in Appendix A shows how all these effects are present in a realistic molecular description. This latter effect is *not* present in our formulation due to the neglect of the memory matrix φ [Eq. (A13)]. An appropriate treatment of φ should introduce nondiffusive, solvent viscosity independent corrections.

There is some arbitrariness in the determination of the Rouse shift parameter θ (see Sec. V), but the choice given provides a good fit of our model. Effects due to hydrodynamic interactions must also be included. The latter are not expected to change any qualitative features of the model. It is of interest to use the model to derive an expression for exact internal friction of a Rouse-like (or Rouse-Zimm-like) chain as a function of γ, ϵ_1, ϵ_2, etc. The last two of these will be presented in subsequent papers.

ACKNOWLEDGMENTS

We are grateful to Professor John Schrag for his continued encouragement in this work and to Professor John Ferry and Professor Walter Stockmayer for helpful discussions. This research is supported, in part, by NSF Grant DMR78-26630 (polymers program).

APPENDIX A

We consider a generalized linear homopolymer of the form

$$\begin{bmatrix} Y \\ | \\ X \end{bmatrix}_{N+1} \equiv \begin{matrix} Y_0 & Y_1 & & & Y_N \\ | & | & & & | \\ X_0 - & X_1 - & \cdot & \cdot \cdot & - X_N \end{matrix}, \tag{A1}$$

where X and Y correspond to a particular decomposition of individual (or groups of) monomers into "backbone" and "sidegroup" units, respectively.[24] For a given monomer, several such decompositions may be possible. The αth partition is designated by the groups X_α and Y_α. Their constituent atoms are denoted by position and momentum coordinates $\{\mathbf{x}^i_\alpha, \mathbf{p}^i_{x\alpha}; i \in X_\alpha\}$ and $\{\mathbf{y}^i_\alpha, \mathbf{p}^i_{y\alpha}; i \in Y_\alpha\}$, respectively, and their masses are m_{xi} and m_{yi}, respectively.

In the free draining limit, the dynamical behavior of this system is governed by the following Fokker-Planck equation for the polymer distribution function $f(t)$:

$$\frac{\partial}{\partial t} f(t) = \Bigg[- \sum_{\alpha, i \in X_\alpha} \left(m^{-1}_{xi} \frac{\partial}{\partial \mathbf{x}^i_\alpha} \cdot \mathbf{p}^i_{x\alpha} - \frac{\partial U}{\partial \mathbf{x}^i_\alpha} \cdot \frac{\partial}{\partial \mathbf{p}^i_{x\alpha}} \right) - \sum_{\alpha, i \in Y_\alpha} \left(m^{-1}_{yi} \frac{\partial}{\partial \mathbf{y}^i_\alpha} \cdot \mathbf{p}^i_{y\alpha} - \frac{\partial U}{\partial \mathbf{y}^i_\alpha} \cdot \frac{\partial}{\partial \mathbf{p}^i_{y\alpha}} \right)$$

$$+ \sum_{\alpha, i \in X_\alpha} \frac{\partial}{\partial \mathbf{p}^i_{x\alpha}} \cdot k_B T \zeta_{xi} \left(\frac{\partial}{\partial \mathbf{p}^i_{x\alpha}} + \frac{1}{k_B T} \mathbf{p}^i_{x\alpha} \right) + \sum_{\alpha, i \in Y_\alpha} \frac{\partial}{\partial \mathbf{p}^i_{y\alpha}} \cdot k_B T \zeta_{yi} \left(\frac{\partial}{\partial \mathbf{p}^i_{y\alpha}} + \frac{1}{k_B T} \mathbf{p}^i_{y\alpha} \right) \Bigg] f(t) , \tag{A2a}$$

or more concisely as

$$\frac{\partial}{\partial t} f(t) = \mathfrak{M} f(t) , \tag{A2b}$$

where ζ_{xi} and ζ_{yi} represent the friction coefficients for the ith particles in X_α and Y_α. U is the total potential of mean force including both bonding and nonbonding (steric and excluded volume) interactions.

The mean evolution of a dynamical vairable A ($\{\mathbf{x}^i_\alpha, \mathbf{p}^i_{x\alpha}, \mathbf{y}^i_\alpha, \mathbf{p}^i_{y\alpha}\}$) is given by

$$\langle A(t)\rangle = \int \prod_{\alpha} \prod_{\substack{i\in X_\alpha \\ j\in Y_\alpha}} d\mathbf{x}_\alpha^i \, d\mathbf{p}_{x\alpha}^i \, d\mathbf{y}_\alpha^j \, d\mathbf{p}_{y\alpha}^j A \, e^{t\mathfrak{M}} f(0) , \quad \text{(A3a)}$$

which is conveniently reexpressed as

$$\langle A(t)\rangle = \int \prod_{\alpha} \prod_{\substack{i\in X_\alpha \\ j\in Y_\alpha}} d\mathbf{x}_\alpha^i \, d\mathbf{p}_{x\alpha}^i \, d\mathbf{y}_\alpha^j \, d\mathbf{p}_{y\alpha}^j f(0) \, e^{t\mathfrak{L}} A , \quad \text{(A3b)}$$

where $\mathfrak{L}$ is the adjoint operator of $\mathfrak{M}$. Thus, the determination of $\langle A(t)\rangle$ is equivalent to first evaluating.

$$A(t) \equiv e^{t\mathfrak{L}} A(0) , \quad \text{(A4a)}$$

$$\frac{\partial}{\partial t} A(t) = \mathfrak{L} A(t) , \quad \text{(A4b)}$$

and then performing an average with respect to $f(0)$. Equation (A4) has the advantage of being immediately amenable to projection operator techniques, a point which has proven to be useful in applications to polymer dynamics and other areas of statistical mechanics.

Bixon and Zwanzig[19,20] have already shown how the Rouse–Zimm model emerges from the general dynamics of a backbone only chain (no Y units) when projection operator formalisms[30,31] are utilized and the resultant memory functions are ignored. Thus, it is clear that all deviations from Rouse–Zimm behavior can, in principle, be expressed in terms of these memory functions. A calculation of the latter is given for a backbone only chain by Adelman and Freed,[9] and the results provide considerable insight into the nature of intrachain friction processes. However, the theoretical methods for calculating memory functions are valid only in the low frequency limit, so they cannot be utilized at frequencies relevant to the plateau viscosity region, etc., which are experimentally relevant, without a considerable amount of numerical analysis. Within the projection operator formalism, an alternative (or equivalent) to the evaluation of memory functions is the specification of the additional "relevant" or slowest set of dynamical variables. It is in this spirit that this Appendix and the model are presented. The viscoelastic experiments of Ferry, Schrag, and co-workers[4,5] strongly suggest a relationship between the value of the plateau viscosity and side group flexibility and motion. Thus, we take the side group variables to be the relevant ones in addition to the backbone variables considered by Bixon and Zwanzig.

In order to relate this generalized dynamical model to the A–B model discussed in the body of the paper, we identify the coordinates $\{\mathbf{x}_\alpha, \mathbf{y}_\alpha\}$ as being, respectively, center of mass coordinates for X_α and Y_α:

$$\mathbf{x}_\alpha \equiv \frac{1}{m_x} \sum_{i\in X_\alpha} m_{xi} \mathbf{x}_\alpha^i , \quad m_x \equiv \sum_{\substack{i\in X_\alpha \\ \text{any } \alpha}} m_{xi} , \quad \text{(A5a)}$$

$$\mathbf{y}_\alpha \equiv \frac{1}{m_y} \sum_{j\in Y_\alpha} m_{yi} \mathbf{y}_\alpha^i , \quad m_y \equiv \sum_{\substack{j\in Y_\alpha \\ \text{any } \alpha}} m_{yj} . \quad \text{(A5b)}$$

The corresponding center of mass momenta are $\mathbf{p}_{x\alpha} \equiv \sum_{i\in X_\alpha} \mathbf{p}_{x\alpha}^i$, $\mathbf{p}_{y\alpha} \equiv \sum_{i\in Y_\alpha} \mathbf{p}_{y\alpha}^j$.

Defining the projection operator $\mathcal{P}$ as

$$\mathcal{P} G \equiv \langle G\mathbf{A}\rangle \cdot \langle \mathbf{A}\mathbf{A}^T\rangle^{-1} \cdot \mathbf{A} , \quad G \text{ arbitrary} , \quad \text{(A6)}$$

where $\mathbf{A}$ represents a column vector of the relevant variables (T is transpose),

$$\mathbf{A} \equiv \mathrm{col}[\{\mathbf{x}_\alpha, \mathbf{p}_{x\alpha}, \mathbf{y}_\alpha, \mathbf{p}_{y\alpha}\}] , \quad \text{(A7)}$$

$$\langle\{\}\rangle \equiv \int \prod_{\alpha} \prod_{\substack{i\in X_\alpha \\ j\in Y_\alpha}} d\mathbf{x}_\alpha^i \, d\mathbf{p}_{x\alpha}^i \, d\mathbf{y}_\alpha^j \, d\mathbf{p}_{y\alpha}^j \{\} \exp\left[-\frac{1}{k_B T}\left(U + \sum_{\alpha, i\in X_\alpha} (\mathbf{p}_{x\alpha}^i)^2/2m_{xi} + \sum_{\alpha, j\in Y_\alpha} (\mathbf{p}_{y\alpha}^j)^2/2m_{yj}\right)\right] \Bigg/$$

$$\int \prod_{\alpha} \prod_{\substack{i\in X_\alpha \\ j\in Y_\alpha}} d\mathbf{x}_\alpha^i \, d\mathbf{p}_{x\alpha}^i \, d\mathbf{y}_\alpha^j \, d\mathbf{p}_{y\alpha}^j \exp\left[-\frac{1}{k_B T}\left(U + \sum_{\alpha, i\in X_\alpha} (\mathbf{p}_{x\alpha}^i)^2/2m_{xi} + \sum_{\alpha, j\in Y_\alpha} (\mathbf{p}_{y\alpha}^j)^2/2m_{yj}\right)\right] . \quad \text{(A8)}$$

Applying standard projection operator techniques[31] results in

$$\frac{d}{dt}\mathbf{x}_\alpha(t) = m_x^{-1} \mathbf{p}_{x\alpha}(t) , \quad \text{(A9)}$$

$$\frac{d}{dt}\mathbf{y}_\alpha(t) = m_y^{-1} \mathbf{p}_{y\alpha}(t) , \quad \text{(A10)}$$

$$\frac{d}{dt}\mathbf{p}_{y\alpha}(t) = -m_y^{-1}\left(\sum_{j\in Y} \zeta_{yj}\right)\mathbf{p}_{y\alpha}(t) - k_B T \sum_{\beta}[\boldsymbol{\Gamma}_{\alpha\beta}^{yx} \cdot \mathbf{x}_\beta(t) + \boldsymbol{\Gamma}_{\alpha\beta}^{yy} \cdot \mathbf{y}_\beta(t)]$$
$$+ \int_0^t d\tau \sum_{\beta}[\boldsymbol{\varphi}_{\alpha\beta}^{yx}(t-\tau) \cdot \mathbf{p}_{x\beta}(\tau) + \boldsymbol{\varphi}_{\alpha\beta}^{yy}(t-\tau) \cdot \mathbf{p}_{y\beta}(\tau)] + \mathfrak{F}_{y\alpha}(t) , \quad \text{(A11)}$$

$$\frac{d}{dt}\mathbf{p}_{x\alpha}(t) = -m_x^{-1}\left(\sum_{i\in X} \zeta_{xi}\right)\mathbf{p}_{x\alpha}(t) - k_B T \sum_{\beta}[\boldsymbol{\Gamma}_{\alpha\beta}^{xx} \cdot \mathbf{x}_\beta(t) + \boldsymbol{\Gamma}_{\alpha\beta}^{xy} \cdot \mathbf{y}_\beta(t)]$$
$$+ \int_0^t d\tau \sum_{\beta}[\boldsymbol{\varphi}_{\alpha\beta}^{xx}(t-\tau) \cdot \mathbf{p}_{x\beta}(\tau) + \boldsymbol{\varphi}_{\alpha\beta}^{xy}(t-\tau) \cdot \mathbf{p}_{y\beta}(\tau)] + \mathfrak{F}_{x\alpha}(t) , \quad \text{(A12)}$$

$$\boldsymbol{\varphi}_{\alpha\beta}^{\mu\nu}(t) = \sum_{\substack{\gamma=0 \\ \sigma=x,y}}^{N} \langle \mathfrak{F}_{\mu\alpha}(t) \mathfrak{F}_{\sigma\gamma}(0)\rangle \cdot \boldsymbol{\Gamma}_{\gamma\beta}^{\sigma\nu} , \quad \text{(A13)}$$

$$\begin{bmatrix}\mathfrak{F}_{x\alpha}(t)\\ \mathfrak{F}_{y\alpha}(t)\end{bmatrix} = e^{t(1-\not{P})\mathfrak{L}}(1-\not{P})\mathfrak{L}\begin{bmatrix}\mathbf{p}_{x\alpha}\\ \mathbf{p}_{y\alpha}\end{bmatrix} . \tag{A.14}$$

$\Gamma^{\sigma\nu}_{\gamma\beta}$ refers to the (γ,β) component of the (σ,ν) block in the inverse equilibrium correlation function matrix $\langle \mathrm{col}\{\mathbf{x}_\alpha, \mathbf{y}_\alpha\}\, \mathrm{row}\{\mathbf{x}_\alpha, \mathbf{y}_\alpha\}\rangle^{-1}$.

From Eqs. (A11) and (A12), we immediately make the indentifications of the A and B unit friction coefficients as the sum of their constituent contributions

$$\zeta_A \equiv \sum_{\substack{j\in Y_\alpha \\ \text{any } \alpha}} \zeta_{yj} , \quad \zeta_B \equiv \sum_{\substack{i\in X_\alpha \\ \text{any } \alpha}} \zeta_{xi} . \tag{A15}$$

Neglect of the "random forces" $\{\mathfrak{F}^{\mu\nu}_{\alpha\beta}\}$ is equivalent to ignoring internal motions within X and Y groups, and the effects of nonlinear contributions to U. Furthermore, if we confine ourselves to motions on time scales satisfying $t \gg \zeta_A^{-1}$, $t \gg \zeta_B^{-1}$, then the inertial terms in Eqs. (A11) and (A12) may also be neglected. With these simplications, Eqs. (A9)–(A12) reduce to

$$\frac{d}{dt}\mathbf{x}_\alpha(t) = k_B T \zeta_B^{-1} \sum_\beta [\Gamma^{xx}_{\alpha\beta} \circ \mathbf{x}_\beta(t) + \Gamma^{xy}_{\alpha\beta} \circ \mathbf{y}_\beta(t)] , \tag{A16a}$$

$$\frac{d}{dt}\mathbf{y}_\alpha(t) = k_B T \zeta_A^{-1} \sum_\beta [\Gamma^{yx}_{\alpha\beta} \circ \mathbf{x}_\beta(t) + \Gamma^{yy}_{\alpha\beta} \cdot \mathbf{y}_\beta(t)] , \tag{A16b}$$

from which explicit microscopic expressions for the constants σ_B, ϵ_1, ϵ_2, ϵ_3, etc. may be identified.

In view of the earlier works of Zwanzig and Bixon, Eq. (A16) is not at all surprising. Note that Eq. (A16), in general, contains interactions between non-nearest neighbors, including those long range interactions (along a chain) invoked by deGennes[29] to obtain the original form of the Cerf theory[7] with internal viscosity independent of solvent viscosity. As the viscoelastic and dielectric experiments of interest to us are in the solvent viscosity limited regime, we concentrate in this paper on the effects of the short range interactions since these appear to be more relevant to the experiments of interest.

APPENDIX B

The transformation matrix $\Phi_{k\alpha}(j)$ [Eq. (3.2)] is determined as a solution to the following eigenvalue problem:

$$\begin{pmatrix}1 & 0\\ 0 & \gamma\end{pmatrix}\cdot\sum_{j=0}^{N}\left[\begin{pmatrix}1-\frac{1}{2}\epsilon_2 & \epsilon_2/2\\ \epsilon_2/2 & -\epsilon_2/2\end{pmatrix}A_{ij} - (\epsilon_1+\epsilon_2)\begin{pmatrix}1 & -1\\ -1 & 1\end{pmatrix}\delta_{ij}\right]$$

$$\cdot\,\Phi_{k\alpha}(j) = -\lambda_{k\alpha}\Phi_{k\alpha}(i) , \tag{B1a}$$

which is written more conveniently as

$$\Lambda\cdot\Phi_{k\alpha}(j) = -\lambda_{k\alpha}\Phi_{k\alpha}(j) , \tag{B1b}$$

and which may be considered the defining relation for the operator Λ. From the endpoint equations of motion [Eq. (3.1)], the $\{\Phi_{k\alpha}(j)\}$ must satisfy

$$\begin{pmatrix}1 & 0\\ 0 & 0\end{pmatrix}\circ\Phi_{k\alpha}(0) - \begin{pmatrix}0 & -1\\ -1 & 1\end{pmatrix}\cdot\Phi_{k\alpha}(-1) = \mathbf{0} , \tag{B2a}$$

$$\begin{pmatrix}1 & 0\\ 0 & 0\end{pmatrix}\circ\Phi_{k\alpha}(N) - \begin{pmatrix}0 & -1\\ -1 & 1\end{pmatrix}\cdot\Phi_{k\alpha}(N+1) = \mathbf{0} . \tag{B2b}$$

The solution of Eq. (B1) displays the general structure

$$\Phi(j) \sim \begin{bmatrix}A\\ B\end{bmatrix}\exp(i\theta j) , \tag{B3}$$

where the (k,α) subscript is suppressed for brevity. Substituting Eq. (B3) into (B1) results in a secular equation for the coefficients A and B given by

$$\begin{pmatrix}(1-\epsilon_2/2)4\sin^2\frac{\theta}{2} + \epsilon_1 + \epsilon_2 - \lambda & \epsilon_2\left(4\sin^2\frac{\theta}{2}\right)\Big/2 - (\epsilon_1+\epsilon_2)\\ \gamma\left[\epsilon_2\left(4\sin^2\frac{\theta}{2}\right)\Big/2 - (\epsilon_1+\epsilon_2)\right] & \gamma\left[-\epsilon_2\left(4\sin^2\frac{\theta}{2}\right)\Big/2 + \epsilon_1 + \epsilon_2\right] - \lambda\end{pmatrix}\cdot\begin{pmatrix}A\\ B\end{pmatrix} = \begin{pmatrix}0\\ 0\end{pmatrix} . \tag{B4}$$

Nontrivial solutions to Eq. (B4) exist, therefore, when θ takes on either of two possible values for a given λ:

$$4\sin^2(\theta/2) = \frac{1}{\gamma\epsilon_2}\left\{\gamma(\epsilon_1+\epsilon_2) - \lambda\left[1 - \frac{\epsilon_2}{2}(1+\gamma)\right]\right\} \pm \frac{1}{\gamma\epsilon_2}\left(\left\{\gamma(\epsilon_1+\epsilon_2) - \lambda\left[1-\frac{\epsilon_2}{2}(1+\gamma)\right]\right\}^2 + 2\lambda\gamma\epsilon_2[\lambda - (1+\gamma)(\epsilon_1+\epsilon_2)]\right)^{1/2} . \tag{B5}$$

The general solution to Eq. (B1) is given by

$$\Phi(j) = \begin{pmatrix}A\\ B\end{pmatrix}[\exp(i\theta_+ j) + a\exp(-i\theta_+ j) + b\exp(i\theta_- j) + c\exp(-i\theta_- j)] ,$$

which upon substitution into Eq. (B2) results in

$$\cos\left(\frac{N-1}{2}\theta_+\right)\cos\left(\frac{N+1}{2}\theta_-\right) = \cos\left(\frac{N-1}{2}\theta_-\right)\cos\left(\frac{N+1}{2}\theta_+\right) . \tag{B6}$$

Therefore, an exact solution of the eigenvalue problem requires that we first solve the messy transcedental equations (B6) and (B5). An alternative approach, given in Appendix C, provides the solutions to Eq. (B1b) as expansions in N^{-1}.

APPENDIX C

I. Expansion in terms of Rouse modes

Equation (B1) may be written as

$$\Lambda'\cdot\Phi_{k\alpha}(j) + \delta\Lambda\cdot\Phi_{k\alpha}(j) = -\lambda_{k\alpha}\Phi_{k\alpha}(j) , \tag{C1}$$

where the end effect matrix is

$$\delta\Lambda \cdot \Phi_{k\alpha}(j) \equiv \epsilon_2 \sum_{i=0}^{N} \begin{pmatrix} 1 & 0 \\ 0 & \gamma \end{pmatrix} \cdot \begin{pmatrix} 1 & -1 \\ -1 & 1 \end{pmatrix} \delta_{ij}(\delta_{j0} + \delta_{jN}) \cdot \Phi_{k\alpha}(i) , \quad \text{(C2)}$$

and $\Lambda' \equiv \Lambda - \delta\Lambda$ is an operator whose eigenvectors $\{\Phi_{k\alpha}(j)\}$ satisfy the new boundary conditions:

$$\Phi^{(0)}_{k\alpha}(0) - \Phi^{(0)}_{k\alpha}(-1) = 0 , \quad \text{(C3a)}$$

$$\Phi^{(0)}_{k\alpha}(N) - \Phi^{(0)}_{k\alpha}(N+1) = 0 . \quad \text{(C3b)}$$

The operator $\delta\Lambda$ is due only to the presence of side groups on the chain endpoints. Equation (C1) can now be solved perturbatively, treating $\delta\Lambda$ as the perturbation. Equations (C1)–(C3) physically correspond to adding and subtracting

$$\delta U = -\frac{3k_B T}{2\sigma_B^2}\epsilon_2[(\mathbf{x}_0 - \mathbf{y}_0)^2 + (\mathbf{x}_N - \mathbf{y}_N)^2] \quad \text{(C4)}$$

from the free energy U [Eq. (2.1)].

Consider the zeroth order problem

$$\Lambda' \cdot \Phi^{(0)}_{k\alpha}(j) = -\lambda^{(0)}_{k\alpha}\Phi^{(0)}_{k\alpha}(j) , \quad \text{(C5)}$$

subject to the boundary conditions (C3). Equation (C5) is easily solved in form

$$\Phi^{(0)}_{k\alpha}(j) = \begin{bmatrix} A_{k\alpha} \\ B_{k\alpha} \end{bmatrix} \cos\frac{\pi k}{N+1}(j+\tfrac{1}{2}) , \quad \text{(C6)}$$

resulting in the eigenvalue equation for $\lambda^{(0)}_{k\alpha}$:

$$\begin{pmatrix} (1-\epsilon_2/2)\lambda^*_k + \epsilon_1 + \epsilon_2 - \lambda^{(0)}_{k\alpha} & \epsilon_2\lambda^*_k/2 - (\epsilon_1+\epsilon_2) \\ \gamma[\epsilon_2\lambda^*_k/2 - (\epsilon_1+\epsilon_2)_k & \gamma(-\epsilon_2\lambda^*_k/2 + \epsilon_1 + \epsilon_2) - \lambda^{(0)}_{k\alpha} \end{pmatrix} \cdot \begin{pmatrix} A_{k\alpha} \\ B_{k\alpha} \end{pmatrix} = \begin{pmatrix} 0 \\ 0 \end{pmatrix} , \quad \text{(C7)}$$

where $\{\lambda^*_k\}$ are the Rouse eigenvalues [Eq. (3.5c)]. In fact, $\delta\Lambda$ and δU are designed so as to give the zeroth order solution (C6). The solutions for $\{\lambda^{(0)}_{k\alpha}\}$, obtained from the secular equation (C7), are given by Eq. (3.6). Apart from an overall normalization, $A_{k\alpha}$ may be set equal to unity, in which case $B_{k\alpha} \equiv E_{k\alpha}$ [Eq. (3.5b)]. The $\{\Phi^{(0)}_{k\alpha}(j)\}$ are then given by

$$\Phi^{(0)}_{k\alpha}(j) = N_{k\alpha}\begin{pmatrix} 1 \\ E_{k\alpha} \end{pmatrix} \cos\frac{\pi k}{N+1}(j+\tfrac{1}{2}) , \quad \text{(C8)}$$

$N_{k\alpha}$ being the normalization constant. The latter is obtained by requiring that the $\{\Phi^{(0)}_{k\alpha}(j)\}$ be orthonormal with respect to an appropriately defined inner product. Defining

$$(\Psi, \Psi') \equiv \sum_{j=0}^{N} \Psi^T(j) \cdot \begin{pmatrix} 1 & 0 \\ 0 & \gamma^{-1} \end{pmatrix} \cdot \Psi'(j) , \quad \text{(C9)}$$

where $\Psi(j)$ and $\Psi'(j)$ satisfy the boundary conditions (C3), and enables the establishment of the hermiticity of the operator Λ':

$$(\Lambda' \cdot \Psi, \Psi') = (\Psi, \Lambda' \cdot \Psi') . \quad \text{(C10)}$$

With the aid of Eqs. (C8)–(C10) and (3.6) and the distinctness of the $\{\lambda^{(0)}_{k\alpha}\}$, it is straightforward to show that

$$(\Phi^{(0)}_{k\alpha}, \Phi^{(0)}_{k'\alpha'}) = \delta_{kk'}\delta_{\alpha\alpha'} , \quad \text{(C11)}$$

provided that $N_{k\alpha}$ is chosen as

$$N_{k\alpha} = (1+\gamma^{-1}E^2_{k\alpha})^{-1/2}\sqrt{\frac{2}{N+1}} . \quad \text{(C12)}$$

Combining Eqs. (C8) and (C12) results in Eq. (3.5a).

The higher order corrections to $\lambda^{(0)}_{k\alpha}$ are determined using standard Rayleigh–Schrödinger perturbation theory.[32] The first two corrections to $\lambda^{(0)}_{k\alpha}$ are given by

$$\lambda^{(1)}_{k\alpha} = (\Phi^{(0)}_{k\alpha}, \delta\Lambda \cdot \Phi^{(0)}_{k\alpha}) = \frac{4\epsilon_2}{N+1}\frac{(E_{k\alpha}-1)^2}{(1+\gamma^{-1}E^2_{k\alpha})}\cos^2\left[\frac{\pi k}{2(N+1)}\right] , \quad \text{(C13)}$$

$$\lambda^{(2)}_{k\alpha} = \sum_{k',\alpha' \neq k,\alpha} \frac{(v_{k\alpha,k'\alpha'})^2}{\lambda^{(0)}_{k\alpha} - \lambda^{(0)}_{k'\alpha'}} , \quad \text{(C14)}$$

where

$$v_{k\alpha,k'\alpha'} \equiv \frac{\epsilon_2}{N+1}[1+(-1)^{k+k'}]\frac{(E_{k\alpha}-1)(E_{k'\alpha'}-1)}{(1+\gamma^{-1}E^2_{k\alpha})^{1/2}(1+\gamma^{-1}E^2_{k'\alpha'})^{1/2}} \times \cos\left[\frac{\pi k}{2(N+1)}\right]\cos\left[\frac{\pi k'}{2(N+1)}\right] . \quad \text{(C15)}$$

Higher order terms involve powers of $v_{k\alpha,k'\alpha'}$ and hence higher powers of N^{-1}. It should be noted that, for certain choices of ϵ_1, ϵ_2, and γ, there can exist modes (k, α) and $k', \alpha')$ such that $\lambda^{(0)}_{k\alpha} \simeq \lambda^{(0)}_{k'\alpha'}$. This difficulty requires that these almost degenerate modes be combined and treated using quasidegenerate perturbation theory. The resulting series still involve powers of N^{-1}. No such complication arises in the present calculation. For example, the evaluation of $\{\lambda^{(2)}_{k\alpha}\}$ for the parameters chosen in Fig. 5 indicates that $\lambda^{(2)}_{k\alpha}/\lambda^{(0)}_{k\alpha} \sim 10^{-3}$–$10^{-8}$. The additional $1/N$ corrections to the figures from the $\lambda^{(1)}_{k\alpha}$ have been ignored as we are not interested in the magnitude of these corrections.

II. Expansion in terms of side group modes

The evaluation of $\chi_{AA}(\omega)$ requires that we pay specific attention to the side groups at the ends of the chain. In order to do so, Eq. (B1) is rewritten as

$$\Lambda'' \cdot \Phi_{k\alpha}(j) + \delta\Lambda' \cdot \Phi_{k\alpha}(j) = -\lambda_{k\alpha}\Phi_{k\alpha}(j) , \quad \text{(C16)}$$

$$\delta\Lambda' \cdot \Phi_{k\alpha}(j) \equiv \sum_{i=0} \begin{pmatrix} 1 & 0 \\ 0 & \gamma \end{pmatrix} \cdot \begin{pmatrix} 1 & 0 \\ 0 & 0 \end{pmatrix} \delta_{ij}(\delta_{jN} + \delta_{j0}) \cdot \Phi_{k\alpha}(i) . \quad \text{(C17)}$$

The $\{\Phi^{(0)}_{k\alpha}(j)\}$ are now chosen to satisfy

$$\Phi^{(0)}_{k\alpha}(-1) = 0 , \quad \text{(C18a)}$$

$$\Phi^{(0)}_{k\alpha}(N+1) = 0 . \quad \text{(C18b)}$$

Following the same procedure as before, we solve Eq. (C15) perturbatively subject to the boundary conditions given in Eq. (C17). Denoting the zeroth order eigenvectors as $\{\Phi^{(0)}_{k\alpha}\}$ again, the zeroth order solution to Eq. (C16) is of the form

$$\Phi^{(0)}_{k\alpha}(j) = \begin{bmatrix} A_{k\alpha} \\ B_{k\alpha} \end{bmatrix} \sin\frac{\pi k}{(N+2)}(j+1) . \quad \text{(C19)}$$

Applying a similar set of arguments as those which led to Eqs. (3.5) and (3.6) results in

$$\Phi^{(0)}_{k\alpha}(j)=\sqrt{\frac{2}{N+1}}(1+\gamma^{-1}\mathcal{G}^2_{k\alpha})^{-1/2}\begin{pmatrix}1\\ \mathcal{G}_{k\alpha}\end{pmatrix}\sin\frac{\pi k}{N+2}(j+1)\,,$$
$$k=1,2,\ldots,N+1\,, \qquad \text{(C20)}$$

$$\mathcal{G}_{k\alpha}\equiv 1+(\eta^*_k-\eta^{(0)}_{k\alpha})/(-\epsilon_2\eta^*_k/2+\epsilon_1+\epsilon_2)\,, \qquad \text{(C21)}$$

$$\eta^{(0)}_{k\pm}\equiv\frac{1}{2}\left[\left(1-\frac{\epsilon_2}{2}(1+\gamma)\right)\eta^*_k+(1+\gamma)(\epsilon_1+\epsilon_2)\right]$$
$$\pm\frac{1}{2}\left(\left\{\left[1-\frac{\epsilon_2}{2}(1+\gamma)\right]\eta^*_k+(1+\gamma)(\epsilon_1+\epsilon_2)\right\}^2\right.$$
$$\left.-4\gamma\eta^*_k(\epsilon_2\eta^*_k/2+\epsilon_1+\epsilon_2)\right)^{1/2}\,, \qquad \text{(C22)}$$

and

$$\eta^*_k\equiv 4\sin^2\left[\frac{\pi k}{2(N+2)}\right]\,. \qquad \text{(C23)}$$

The leading corrections to Eq. (C21) again involve powers of N^{-1}. For example, $\eta^{(1)}_{k\alpha}$ is given by

$$\eta^{(1)}_{k\alpha}=\frac{4}{N+2}\frac{(\mathcal{G}_{k\alpha}-1)^2}{(1+\gamma^{-1}\mathcal{G}^2_{k\alpha})}\sin^2\left(\frac{\pi k}{N+2}\right)\,. \qquad \text{(C24)}$$

Comparison of Eqs. (C21) and (3.6) indicates that

$$\eta^{(0)}_{k\alpha}=\lambda^{(0)}_{k\alpha}+O(N^{-1})\,,$$

demonstrating that the relaxation spectrum is rather insensitive to the manner in which their calculation is formulated [i.e., Eq. (C1) or (C15)].

According to Eqs. (3.2) and (C19), the vector S [Eq. (5.7)] is expanded as

$$\mathbf{S}(t)=\sqrt{\frac{2}{N+1}}\sum_{\substack{k=1\\ \alpha=\pm\\ k\ \text{odd}}}^{N+1}\cot\left[\frac{\pi k}{2(N+2)}\right]$$
$$\times\frac{\mathcal{G}_{k\alpha}-1}{(1+\gamma^{-1}\mathcal{G}^2_{k\alpha})^{1/2}}\exp\left(-\frac{3k_BT\eta^{(0)}_{k\alpha}t}{\sigma_B^2\zeta_B}\right)\zeta_{k\alpha}\,. \qquad \text{(C25)}$$

APPENDIX D

Consider Eq. (4.5):

$$I=\sum_{k=1}^{N}P_n(\lambda^*_k)/L_m(\lambda^*_k)\,,$$

where P_n and L_m are polynomials of degree n and m, respectively, and $n<m$. We further assume that (i) the roots of L_m are distinct and nonzero, (ii) the roots of P_n and L_m do not coincide, and (iii) the coefficient of $(\lambda^*_k)^m$ is unity. None of these assumptions is a restriction on the applicability of the techniques to be discussed below.

Let the roots of L_m be denoted as $\{4\sin^2\phi_p\}_{p=1}^m$; then I may be rewritten as a partial fraction expansion as

$$I=\sum_{p=1}^{m}I_p\prod_{l\neq p}\frac{P_n(4\sin^2\phi_p)}{4(\sin^2\phi_p-\sin^2\phi_l)}\,, \qquad \text{(D1)}$$

$$I_p\equiv\sum_{k=1}^{N}(\lambda^*_k-4\sin^2\phi_p)^{-1}\,. \qquad \text{(D2)}$$

I_p is evaluated using contour integration techniques. A similar sum had previously been considered by Wallis and Maradudin.[33] However, the latter consider a periodic lattice (i.e., ring boundary conditions) in the choice of their contour. The appropriate contour C for the free end boundary conditions is depicted in Fig. 16. We first write for I_p the more symmetric form

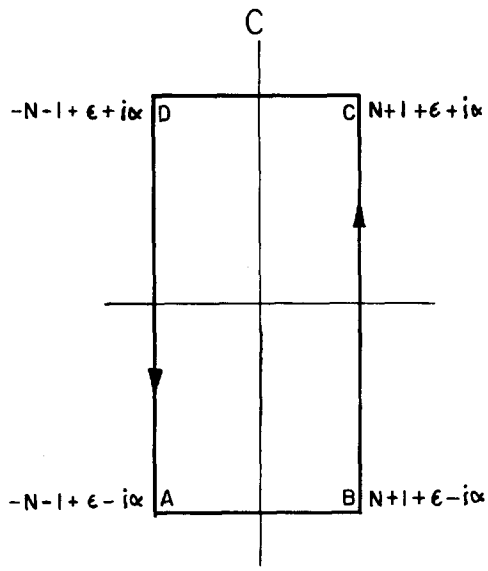

FIG. 16. The contour of integration for Eq. (D3), ϵ is a small positive number and α is ultimately allowed to approach ∞.

$$I_p=\frac{1}{2}\sum_{k=-N}^{N}(\lambda^*_k-4\sin^2\phi_p)^{-1}+\tfrac{1}{2}\cot(2\phi_p)/\sin(2\phi_p)\,,$$

where the last term cancels the added $k=0$ contribution to the sum. Then, taking advantage of the simple poles of $\pi\cot\pi z$ and Cauchy's theorem,[34] it can be verified that I_p is equivalent to

$$I_p=\frac{1}{2}\left(\cot2\phi_p/\sin2\phi_p+\frac{1}{2\pi i}\int_C\frac{\pi\cot\pi z\,dz}{4\left\{\sin^2\left[\frac{\pi z}{2(N+1)}\right]-\sin^2\phi_p\right\}}\right.$$
$$\left.-\text{Res}\frac{\pi\cot\pi z}{4\left\{\sin^2\left[\frac{\pi z}{2(N+1)}\right]-\sin^2\phi_p\right\}}\bigg|_{z=\pm[2(N+1)/\pi]\phi_p}\right)\,, \qquad \text{(D3)}$$

where $|\phi_p|<\pi/2$ if $\text{Im}\phi_p=0$. The remaining analysis proceeds in a similar manner to that of Wallis and Maradudin. The integrals along BC and DA exactly cancel one another, whereas those along AB and CD vanish as $\alpha\to\infty$. As a result, Eq. (D3) reduces to

$$I_p=\frac{1}{2}\left\{\frac{\cot2\phi_p-(N+1)\cot[2(N+1)\phi_p]}{\sin2\phi_p}\right\}\,, \qquad \text{(D4)}$$

and therefore I is given by

$$I=\frac{1}{2}\sum_{p=1}^{m}\prod_{l\neq p}\frac{P_n(4\sin^2\phi_p)}{4(\sin^2\phi_p-\sin^2\phi_l)}$$
$$\times\left\{\frac{\cot2\phi_p-(N+1)\cot[2(N+1)\phi_p]}{\sin2\phi_p}\right\}\,. \qquad \text{(D5)}$$

APPENDIX E

I. Evaluation of $[\eta(\omega)]$

Performing the α summation in Eq. (4.4) results in

$$[\eta(\omega)] = \frac{N_A \zeta_B \sigma_B^2}{6M\eta_0}\left(\sum_{k=1}^{N} \frac{2i\bar{\omega} + \lambda_k^*\left[1 - \frac{\epsilon_2}{2}(1+\gamma)\right] + (1+\gamma)(\epsilon_1+\epsilon_2)}{\frac{1}{2}\epsilon_2\gamma[\lambda_k^* - \eta_+(\bar{\omega})][\lambda_k^* - \eta_-(\bar{\omega})]} + (i\bar{\omega} + \lambda_{0+})^{-1}\right), \tag{E1}$$

where $\eta_\pm$ and $\bar{\omega}$ are defined in Eqs. (4.7) and (4.8), respectively. In order to apply the techniques of Appendix D, we first define

$$4\sin^2\phi_\pm \equiv \eta_\pm(\bar{\omega}), \tag{E2}$$

and

$$P_1(\lambda_k^*) \equiv 2i\bar{\omega} + \lambda_k^*\left[1 - \frac{\epsilon_2}{2}(1+\gamma)\right] + (1+\gamma)(\epsilon_1+\epsilon_2). \tag{E3}$$

Substitution of Eqs. (E2) and (E3) into (D5) and noting the prefactor $(N_A\zeta_B\sigma_B^2)/(3M\eta_0\epsilon_2\gamma)$ gives Eq. (4.6).

II. Evaluation of $\chi_{AA}(\omega)$ and $\chi_{BB}(\omega)$

We note that $\chi_{AA}(\omega)$ and $\chi_{BB}(\omega)$ involve sums over odd values of k. This difficulty is overcome by observing that

$$\sum_{\substack{k=1 \\ k\ \text{odd}}}^{N} f(\lambda_k^*) = \sum_{k=1}^{N} f(\lambda_k^*) - \sum_{k=1}^{(N-1)/2} f\left\{4\sin^2\left[\frac{\pi k}{2\left(\frac{N+1}{2}\right)}\right]\right\}, \quad N\ \text{odd}, \tag{E4}$$

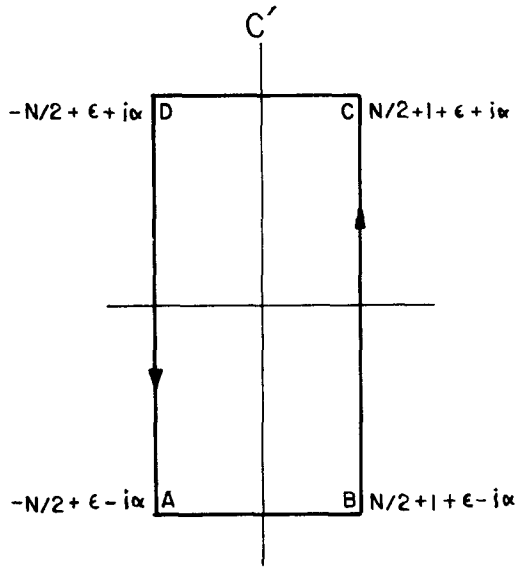

FIG. 17. Contour used to evaluate the sum (E4) for N even.

for which Appendix D is directly applicable. If N is even, then the second term in Eq. (E4) becomes

$$\sum_{k=1}^{N/2} f\left[4\sin^2\left(\frac{\pi k}{N+1}\right)\right],$$

which may be evaluated along the contour displayed in Fig. 17 and using a similar contour integration as before [i.e., Eq. (D3)]. We restrict ourselves to N odd for simplicity.

Performing the α summation in the expression for $\chi_{BB}(\omega)$ [Eq. (5.4)] results in

$$\chi_{BB}(\omega) = -\frac{16\sigma_B^2\mu_B^2}{3\gamma^2\epsilon_2(k_BT)(N+1)} \sum_{\substack{k=1 \\ k\ \text{odd}}}^{N} \cos^2\left[\frac{\pi k}{2(N+1)}\right]\left\{\epsilon_2^2\gamma + \left[1 - \frac{\epsilon_2}{2}(1-\gamma)\right]^2\right\}^{-1}$$
$$\times \frac{\gamma\Delta_k^3 + 2[i\bar{\bar{\omega}}\gamma + \lambda_k^*(1-\gamma)]\Delta_k^2 + (\lambda_k^*)^2(4-3\gamma)\Delta_k + 2(\lambda_k^*)^3}{\prod_{\alpha=\pm}(\lambda_k^* - \delta_\alpha)[\lambda_k^* - \eta_\alpha(\bar{\bar{\omega}})]}, \tag{E5}$$

where $\bar{\bar{\omega}}$ and $\{\eta_\alpha\}$ are defined by Eqs. (5.10) and (4.7), respectively, and

$$\delta_\pm \equiv -(\epsilon_1+\epsilon_2)[-2\gamma \pm i\sqrt{\gamma}\,(1-\gamma)]\left\{\pm i\sqrt{\gamma}\left[1 - \frac{\epsilon_2}{2}(1-\gamma)\right] - \epsilon_2\gamma\right\}^{-1}, \tag{E6}$$

$$\Delta_k \equiv -\frac{\epsilon_2}{2}\lambda_k^* + \epsilon_1 + \epsilon_2. \tag{E7}$$

In order to apply the techniques of Appendix D to Eq. (E5), we first make the identifications

$$P_3(\lambda_k^*) \equiv \gamma\Delta_k^2 + 2[i\bar{\bar{\omega}}\gamma + \lambda_k^*(1-\gamma)]\Delta_k^2 + (\lambda_k^*)^2(4-3\gamma)\Delta_k + 2(\lambda_k^*)^3, \tag{E8a}$$

$$\{4\sin^2\phi_\rho\}_{\rho=1}^4 \equiv \{\eta_+(\bar{\bar{\omega}}), \eta_-(\bar{\bar{\omega}}), \delta_+, \delta_-\}; \tag{E8b}$$

then, $\chi_{BB}(\omega)$ is reduced to

$$\chi_{BB}(\omega) = \frac{-16\sigma_B^2\mu_B^2}{3\gamma^2\epsilon_2 k_B T(N+1)}\left\{\epsilon_2^2\gamma + \left[1 - \frac{\epsilon_2}{2}(1-\gamma)\right]^2\right\}^{-1} \sum_{\rho=1}^{4} \prod_{l\neq\rho} \frac{P_3(4\sin^2\phi_\rho)}{4(\sin^2\phi_\rho - \sin^2\phi_l)} \sum_{\substack{k=1 \\ k\ \text{odd}}}^{N}\left(1 - \frac{\lambda_k^*}{4}\right)(\lambda_k^* - 4\sin^2\phi_\rho)^{-1}$$
$$= -\frac{4\sigma_B^2\mu_B^2}{3\epsilon_2\gamma^2 k_B T}\left\{\epsilon_2^2\gamma + \left[1 - \frac{\epsilon_2}{2}(1-\gamma)\right]^2\right\}^{-1} \sum_{\rho=1}^{4} \prod_{l\neq\rho} \frac{P_3(4\sin^2\phi_\rho)}{4(\sin^2\phi_\rho - \sin^2\phi_l)}\{\cot\phi_\rho \tan[(N+1)\phi_\rho] - \tfrac{1}{2}\}. \tag{E9}$$

The evaluation of $\chi_{AA}(\omega)$ [Eq. (5.8)] proceeds in a similar manner. Defining

$$P_3'(\lambda_k^*) \equiv \Delta_k^2(1+\gamma)^2[\gamma\lambda_k^* + (1+\gamma)i\bar{\bar{\omega}}] + \Delta_k\lambda_k^*[2i\bar{\bar{\omega}}(1+\gamma)(1-2\gamma) - \lambda_k^*\gamma(\gamma^2+9)] + (\lambda_k^*)^2[i\bar{\bar{\omega}}(1-5\gamma-2\gamma^2) - \gamma(1+\gamma)\lambda_k^*] \quad \text{(E10)}$$

enables one to write

$$\chi_{AA}(\omega) = -\frac{16\sigma_B^2\mu_A^2}{\gamma^2\epsilon_2 k_B T(N+1)}\left\{\epsilon_2^2\gamma + \left[1 - \frac{\epsilon_2}{2}(1-\gamma)\right]^2\right\}^{-1} \sum_{\substack{k=1 \\ k \text{ odd}}}^{N} \frac{\cos^2\left[\frac{\pi k}{2(N+1)}\right] P_3'(\lambda_k^*)}{\lambda_k^* \prod_{\alpha=\pm}[\lambda_k^* - \eta_\alpha(\bar{\bar{\omega}})](\lambda_k^* - \delta_\alpha)}, \quad \text{(E11)}$$

where Eq. (E7) has been used. In order to evaluate Eq. (E11), it is convenient to introduce a parameter ϕ_5 such that the lone λ_k^* in the denominator is shifted to $\lambda_k^* - 4\sin^2\phi_5$. The limit $\phi_5 \to 0$ is taken at the end of the calculation. Applying the general principles of Appendix D to Eq. (E11) results in

$$\begin{aligned}\chi_{AA}(\omega) &= -\frac{4\sigma_B^2\mu_A^2}{3\gamma^2\epsilon_2 k_B T}\left\{\epsilon_2^2\gamma + \left[1 - \frac{\epsilon_2}{2}(1-\gamma)\right]^2\right\}^{-1} \lim_{\phi_5 \to 0} \sum_{p=1}^{5} \prod_{l \neq p} \frac{P_3'(4\sin^2\phi_p)}{4(\sin^2\phi_p - \sin^2\phi_l)}\{\cot\phi_p \tan[(N+1)\phi_p] - \tfrac{1}{2}\} \\ &= -\frac{1}{3}\frac{\sigma_B^2\mu_A^2}{\epsilon_2\gamma^2 k_B T}\left\{\epsilon_2^2\gamma + \left[1 - \frac{\epsilon_2}{2}(1-\gamma)\right]^2\right\}^{-1} \sum_{p=1}^{4} \prod_{\substack{l \neq p \\ l \in [1,4]}} \frac{P_3'(4\sin^2\phi_p)}{4(\sin^2\phi_p - \sin^2\phi_l)} \\ &\quad \times \frac{1}{\sin^2\phi_p}\{\cot\phi_p \tan[(N+1)\phi_p] - \tfrac{1}{2}\} + \frac{1}{3}\frac{\sigma_B^2\mu_A^2}{k_B T}\frac{(1+\gamma)(N+\frac{1}{2})}{[i\bar{\bar{\omega}} + (1+\gamma)(\epsilon_1+\epsilon_2)]}. \end{aligned} \quad \text{(E12)}$$

[1] P. E. Rouse, J. Chem. Phys. **21**, 1272 (1953).
[2] B. H. Zimm, J. Chem. Phys. **24**, 269 (1956).
[3] For a review and further references, see H. Yamakawa, *Modern Theory of Polymer Solutions* (Harper and Row, New York, 1971).
[4] J. W. M. Noordermeer, O. Kramer, F. H. M. Nestler, J. L. Schrag, and J. D. Ferry, Macromolecules **8**, 539 (1975); J. W. M. Noordermeer, J. D. Ferry and N. Nemoto, *ibid.* **8**, 672 (1975).
[5] B. G. Brueggman, M. G. Minnick, and J. L. Schrag, Macromolecules **11**, 119 (1978).
[6] W. Kuhn and H. Kuhn, Helv. Chim. Acta **26**, 1394 (1943); **28**, 1533 (1945); **29**, 7, 609, 830 (1946).
[7] R. Cerf, Fortschr. Hochpolymer Forsch. **1**, 382 (1959); Phys. Lett. **16**, 42 (1972); **22**, 613 (1973).
[8] A. Peterlin, J. Polym. Sci. Part A 2 **5**, 179 (1967); J. Polym. Sci. Part B **10**, 101 (1972).
[9] S. A. Adelman and K. F. Freed, J. Chem. Phys. **67**, 1380 (1977).
[10] M. Fixman and J. Kovac, J. Chem. Phys. **61**, 4939, 4950 (1974); **63**, 935 (1975); M. Fixman, G. T. Evans, *ibid.* **64**, 3474 (1976).
[11] M. Doi, H. Nakajima, and Y. Wada, Colloid Polym. Sci. **253**, 905 (1975); **254**, 559 (1976).
[12] M. Fixman, J. Chem. Phys. **68**, 2983 (1978); **69**, 1527, 1538 (1978).
[13] W. H. Stockmayer and K. Matsuo, Macromolecules **5**, 766 (1972).
[14] E. Dubois-Violette, F. Gény, L. Monnerie, and O. Parodi, J. Chim. Phys. **66** (1969).
[15] B. Valeur, J. P. Jarry, F. Gény, and L. Monnerie, J. Polym. Sci. Polym. Phys. Ed. **13**, 2251 (1975).
[16] A. A. Jones and W. H. Stockmayer, J. Polym. Sci. Polym. Phys. Ed. **15**, 847 (1977); K. Matsuo, K. F. Kuhlmann, W. H. Yang, F. Gény, W. H. Stockmayer, and A. A. Jones, *ibid.* **15**, 1347 (1977).
[17] R. S. Adler and K. F. Freed, Macromolecules **11**, 1058 (1978).
[18] M. G. Sheppard, R. S. Adler, and K. F. Freed (to be published).
[19] M. Bixon, J. Chem. Phys. **58**, 1459 (1973).
[20] R. Zwanzig, J. Chem. Phys. **60**, 2717 (1974).
[21] M. Fixman and G. T. Evans, J. Chem. Phys. **68**, 195 (1978).
[22] W. H. Stockmayer, W. Gobush, Y. Chikahisa, and D. K. Carpenter, Discuss. Faraday Soc. **49**, 182 (1970).
[23] J. E. Shore and R. Zwanzig, J. Chem. Phys. **63**, 5445 (1975).
[24] The model and free energy expression (2.1) may not correspond precisely to polystyrene (or any vinyl polymers) where the large phenyl side group is associated with alternate backbone carbon atoms. However, as discussed in Appendix A, there is some freedom in the choice of A and B units with the projection operator method. For example, we may choose

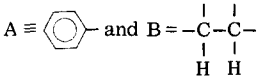

as the fundamental units. Then **y** and **x** refer to their center of mass coordinates, respectively. Neglecting any local anisotropies due to this particular choice of A and B units then results in the form (2.1). The model is readily extended to include two types of backbone units $B = -CH_2-$ and $B' = -\overset{|}{C}H-$, with the side group A attached only to B′ units. The basic calculation remains similar, only now 3×3 matrices and their eigenvalues are involved. The additional complexity is not sufficient to warrant of this more general description until the mathematically simpler case, studied here, is found to be deficient in the explanation of experimental data because of the grosser choice of individual backbone units.
[25] S. Kästner, Kolloid Z. Z. Polym. **184**, 109 (1962).
[26] J. L. Schrag (private communication).
[27] D. A. McQuarrie, *Statistical Mechanics* (Harper and Row, New York, 1976).
[28] S. F. Edwards and A. G. Goodyear, J. Phys. A **5**, 965 (1972).
[29] P. G. deGennes, J. Chem. Phys. **66**, 5825 (1977).
[30] R. Zwanzig, J. Chem. Phys. **33**, 1338 (1960).
[31] H. Mori, Prog. Theor. Phys. (Kyoto) **33**, 423 (1965).
[32] E. Merzbacher, *Quantum Mechanics* (Wiley, New York, 1970).
[33] R. F. Wallis and A. A. Maradudin, Prog. Theor. Phys. (Kyoto) **24**, 1055 (1960).
[34] See, for example, P. Dennery and A. Krzywicki, *Mathematics for Physicists* (Harper and Row, New York, 1967).